

A SYMMETRIZED PARAMETRIC FINITE ELEMENT METHOD FOR ANISOTROPIC SURFACE DIFFUSION OF CLOSED CURVES VIA A CAHN-HOFFMAN ξ -VECTOR FORMULATION

WEIZHU BAO*, WEI JIANG[†], AND YIFEI LI[‡]

Abstract. We deal with a long-standing problem about how to design an energy-stable numerical scheme for solving the motion of a closed curve under *anisotropic surface diffusion* with a general anisotropic surface energy $\gamma(\mathbf{n})$ in two dimensions, where \mathbf{n} is the outward unit normal vector. By introducing a novel symmetric positive definite surface energy matrix $Z_k(\mathbf{n})$ depending on the Cahn-Hoffman ξ -vector and a stabilizing function $k(\mathbf{n})$, we first reformulate the anisotropic surface diffusion into a conservative form and then derive a new symmetrized variational formulation for the anisotropic surface diffusion with weakly or strongly anisotropic surface energies. A semi-discretization in space for the symmetrized variational formulation is proposed and its area (or mass) conservation and energy dissipation are proved. The semi-discretization is then discretized in time by either an implicit structural-preserving scheme (SP-PFEM) which preserves the area in the discretized level or a semi-implicit energy-stable method (ES-PFEM) which needs only solve a linear system at each time step. Under a relatively simple and mild condition on $\gamma(\mathbf{n})$, we show that both SP-PFEM and ES-PFEM are unconditionally energy-stable for almost all anisotropic surface energies $\gamma(\mathbf{n})$ arising in practical applications. Specifically, for several commonly-used anisotropic surface energies, we construct $Z_k(\mathbf{n})$ explicitly. Finally, extensive numerical results are reported to demonstrate the high performance of the proposed numerical schemes.

Key words. Anisotropic surface diffusion, Cahn-Hoffman ξ -vector, anisotropic surface energy, parametric finite element method, structure-preserving, energy-stable, surface energy matrix

AMS subject classifications. 65M60, 65M12, 35K55, 53C44

1. Introduction. Anisotropic surface diffusion is an important and common process at material surfaces/interfaces in solids due to different surface lattice orientations. The lattice orientational difference leads to anisotropic surface energy in solid materials. It thus generates an anisotropic evolution process in both diffusion rates and mechanisms for the varying surface orientations of a material. Recently, anisotropic surface diffusion has been known as important kinetics and/or mechanism in surface phase formation, epitaxial growth, heterogeneous catalysis, and many other areas in surface/materials science [28, 27]. It has proven significant and broader applications in materials science, and computational geometry as well as solid-state physics, such as the evolution of voids in microelectronic circuits [23, 36], microstructure evolution in solids [9, 15], the smoothing of discrete surfaces [11], and solid-state dewetting [31, 38, 18, 32, 26].

As shown in Fig. 1.1, for a closed curve Γ in two dimensions (2D) associated with a given anisotropic surface energy $\gamma(\mathbf{n})$, where $\mathbf{n} = (n_1, n_2)^T \in \mathbb{S}^1$ representing the unit outward normal vector, the motion by anisotropic surface diffusion of the curve is described by the following geometric evolution equation [25, 10]

$$(1.1) \quad v_n = \partial_{ss}\mu,$$

*Department of Mathematics, National University of Singapore, Singapore, 119076 (mat-baowz@nus.edu.sg). This author's research was supported by the Ministry of Education of Singapore grant MOE2019-T2-1-063 (R-146-000-296-112).

[†]School of Mathematics and Statistics & Hubei Key Laboratory of Computational Science, Wuhan University, Wuhan, 430072, P. R. China (jiangwei1007@whu.edu.cn). This author's research was supported by the National Natural Science Foundation of China No. 11871384 and the Fundamental Research Funds for the Central Universities No. 2042021kf1031.

[‡]Department of Mathematics, National University of Singapore, Singapore, 119076 (e0444158@u.nus.edu).

where v_n is the normal velocity, s is the arclength parameter of Γ , and $\mu := \mu(\mathbf{n})$ is the chemical potential (or weighted curvature denoted as $\kappa_\gamma := \kappa_\gamma(\mathbf{n})$ in the literature [29]) generated from the energy functional $W(\Gamma) := \int_\Gamma \gamma(\mathbf{n}) ds$ via the thermodynamic variation [10, 2]. It is well-known that the anisotropic surface diffusion has the following two essential geometric properties: (i) the area of the region enclosed by the curve is conserved, and (ii) the free energy (or weighted perimeter) $W(\Gamma)$ of the curve decreases in time [32, 2]. More precisely, the motion by anisotropic surface diffusion is the H^{-1} -gradient flow of the free energy (or weighted perimeter) functional $W(\Gamma)$ [30, 24]. Let $\gamma(\mathbf{p}) : \mathbb{R}_*^2 := \mathbb{R}^2 \setminus \{\mathbf{0}\} \rightarrow \mathbb{R}^+$ be a homogeneous extension

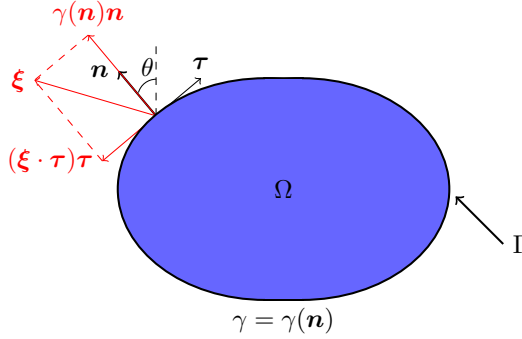


FIG. 1.1. An illustration of a closed curve Γ in \mathbb{R}^2 under anisotropic surface diffusion with an anisotropic surface energy $\gamma(\mathbf{n})$, where \mathbf{n} is the outward unit normal vector, $\boldsymbol{\tau}$ is the unit tangential vector, $\boldsymbol{\xi}$ is the Cahn-Hoffman $\boldsymbol{\xi}$ -vector in (1.3), and θ is the angle between \mathbf{n} and y -axis.

of the anisotropic surface energy $\gamma(\mathbf{n}) : \mathbb{S}^1 \rightarrow \mathbb{R}^+$ satisfying: (i) $\gamma(\mathbf{p})|_{\mathbf{p}=\mathbf{n}} = \gamma(\mathbf{n})$ for $\mathbf{n} \in \mathbb{S}^1$, and (ii) $\gamma(c\mathbf{p}) = c\gamma(\mathbf{p})$ for $c > 0$ and $\mathbf{p} \in \mathbb{R}_*^2$. A typical homogeneous extension is widely used in the literature as [20, 12]

$$(1.2) \quad \gamma(\mathbf{p}) := |\mathbf{p}| \gamma\left(\frac{\mathbf{p}}{|\mathbf{p}|}\right), \quad \forall \mathbf{p} = (p_1, p_2)^T \in \mathbb{R}_*^2 := \mathbb{R}^2 \setminus \{\mathbf{0}\},$$

where $|\mathbf{p}| = \sqrt{p_1^2 + p_2^2}$. Then the Cahn-Hoffman $\boldsymbol{\xi}$ -vector introduced by Cahn and Hoffman is mathematically given by [16, 33]

$$(1.3) \quad \boldsymbol{\xi} := \boldsymbol{\xi}(\mathbf{n}) = \nabla \gamma(\mathbf{p})|_{\mathbf{p}=\mathbf{n}} = \gamma(\mathbf{n})\mathbf{n} + (\boldsymbol{\xi} \cdot \boldsymbol{\tau})\boldsymbol{\tau}, \quad \forall \mathbf{n} \in \mathbb{S}^1,$$

where $\boldsymbol{\tau} = \mathbf{n}^\perp$ is the unit tangential vector with the notation $^\perp$ denoting clockwise rotation by $\frac{\pi}{2}$ (cf. Fig. 1.1). Furthermore, the chemical potential μ (or weighted curvature) and the Hessian matrix $H_\gamma(\mathbf{n})$ are defined as [20]

$$(1.4) \quad \mu := \mu(\mathbf{n}) = -\mathbf{n} \cdot \partial_s \boldsymbol{\xi}^\perp, \quad H_\gamma(\mathbf{n}) := \nabla \nabla \gamma(\mathbf{p})|_{\mathbf{p}=\mathbf{n}}, \quad \forall \mathbf{n} \in \mathbb{S}^1.$$

We remark here that $H_\gamma(\mathbf{n})\mathbf{n} = \mathbf{0}$ and thus 0 is an eigenvalue of $H_\gamma(\mathbf{n})$ and \mathbf{n} is a corresponding eigenvector. We denote the other eigenvalue of $H_\gamma(\mathbf{n})$ as $\lambda(\mathbf{n}) \in \mathbb{R}$.

Let $\Gamma := \Gamma(t)$ be parameterized by $\mathbf{X} := \mathbf{X}(s, t) = (x(s, t), y(s, t))^T \in \mathbb{R}^2$ with t representing the time and s denoting the arclength parametrization of Γ (cf. Fig. 1.1), then via the Cahn-Hoffman $\boldsymbol{\xi}$ -vector in (1.3), the anisotropic surface diffusion

equation (1.1) for Γ is described as follows [20]:

$$(1.5a) \quad \begin{cases} \partial_t \mathbf{X} = \partial_{ss} \mu \mathbf{n}, & 0 < s < L(t), \quad t > 0, \\ \mu = -\mathbf{n} \cdot \partial_s \boldsymbol{\xi}^\perp, \quad \boldsymbol{\xi} = \nabla \gamma(\mathbf{p})|_{\mathbf{p}=\mathbf{n}}, \end{cases}$$

where $L(t) = \int_{\Gamma(t)} ds$ is the perimeter of $\Gamma(t)$, and

$$(1.6) \quad \boldsymbol{\tau} = \partial_s \mathbf{X} = \mathbf{n}^\perp, \quad \mathbf{n} = -\partial_s \mathbf{X}^\perp = -\boldsymbol{\tau}^\perp.$$

The initial data for (1.5) is given as

$$(1.7) \quad \mathbf{X}(s, 0) = \mathbf{X}_0(s) = (x_0(s), y_0(s))^T, \quad 0 \leq s \leq L_0,$$

where L_0 is the perimeter (or length) of the initial curve $\Gamma_0 = \Gamma(0)$.

When $\gamma(\mathbf{n}) \equiv \text{constant}$ (e.g. $\gamma(\mathbf{n}) \equiv 1$), for $\mathbf{n} \in \mathbb{S}^1$, it is also named as *isotropic* surface energy; and in the isotropic case, $\gamma(\mathbf{p}) = |\mathbf{p}|$ in (1.2), $\boldsymbol{\xi} = \mathbf{n}$ in (1.3), and $\mu = \kappa$ and $H_\gamma(\mathbf{n}) \equiv I_2 - \mathbf{n}\mathbf{n}^T$ in (1.4) with κ the curvature and I_2 the 2×2 identity matrix and $\lambda(\mathbf{n}) \equiv 1$, and thus the anisotropic surface diffusion (1.1) collapses to the surface diffusion [5, 25, 21, 40]. In contrast, when $\gamma(\mathbf{n})$ is not a function of a constant value, it is named as *anisotropic* surface energy; and in the anisotropic case, when $\boldsymbol{\tau}^T H_\gamma(\mathbf{n}) \boldsymbol{\tau} > 0$ for all $\mathbf{n} \in \mathbb{S}^1$ with $\boldsymbol{\tau} = \mathbf{n}^\perp$ ($\Leftrightarrow \lambda(\mathbf{n}) > 0$ for $\mathbf{n} \in \mathbb{S}^1$), it is called as *weakly anisotropic*; and when $\boldsymbol{\tau}^T H_\gamma(\mathbf{n}) \boldsymbol{\tau}$ changes sign for $\mathbf{n} \in \mathbb{S}^1$ with $\boldsymbol{\tau} = \mathbf{n}^\perp$ ($\Leftrightarrow \lambda(\mathbf{n})$ changes sign for $\mathbf{n} \in \mathbb{S}^1$), it is called as *strongly anisotropic*. Some commonly-used anisotropic surface energies $\gamma(\mathbf{n})$ in the literature are summarized as below:

(i) the Riemannian metric anisotropic surface energy [6, 8]

$$(1.8) \quad \gamma(\mathbf{n}) = \sqrt{\mathbf{n}^T G \mathbf{n}}, \quad \forall \mathbf{n} \in \mathbb{S}^1,$$

where $G \in \mathbb{R}^{2 \times 2}$ is a symmetric positive definite (SPD) matrix;

(ii) the l^r -norm metric anisotropic surface energy [12]

$$(1.9) \quad \gamma(\mathbf{n}) = \|\mathbf{n}\|_{l^r} = (|n_1|^r + |n_2|^r)^{\frac{1}{r}}, \quad \forall \mathbf{n} = (n_1, n_2)^T \in \mathbb{S}^1,$$

where $1 < r < \infty$;

(iii) the m -fold anisotropic surface energy [3]

$$(1.10) \quad \gamma(\mathbf{n}) = 1 + \beta \cos(m(\theta - \theta_0)), \quad \forall \mathbf{n} = (n_1, n_2)^T = (-\sin \theta, \cos \theta)^T \in \mathbb{S}^1,$$

where $m = 2, 3, 4, 6$, $\theta_0 \in [-\pi, \pi]$ is a constant, and $\beta \geq 0$ is a dimensionless anisotropic strength constant; and

(iv) the regularized l^1 -norm metric anisotropic surface energy which can be viewed as a regularization for the non-smooth surface energy $\gamma(\mathbf{n}) = |n_1| + |n_2|$ [6, 7]

$$(1.11) \quad \gamma(\mathbf{n}) = \sqrt{n_1^2 + \varepsilon^2 n_2^2} + \sqrt{\varepsilon^2 n_1^2 + n_2^2}, \quad \forall \mathbf{n} = (n_1, n_2)^T \in \mathbb{S}^1,$$

where $0 < \varepsilon \ll 1$ is a regularization parameter. For convenience of readers, in Appendix A, we list $\gamma(\mathbf{p})$ via the extension (1.2), $\boldsymbol{\xi}$ in (1.3), and $H_\gamma(\mathbf{n})$ in (1.4) and its eigenvalue $\lambda(\mathbf{n})$ for the above anisotropic surface energies.

Different numerical methods have been proposed for the isotropic/anisotropic surface diffusion, such as the marker-particle method [34, 13], the finite element

method via graph evolution [1, 12], the θ - L formulation method [17], the discontinuous Galerkin finite element method [37], and the parametric finite element method (PFEM) [5, 3, 20, 22]. Among these methods, the PFEM performs the best in terms of accuracy and efficiency as well as mesh quality in practical computations via reformulating (1.5) as [20]

$$(1.12a) \quad \begin{cases} \mathbf{n} \cdot \partial_t \mathbf{X} = \partial_{ss} \mu, & 0 < s < L(t), \quad t > 0, \\ \mu \mathbf{n} = -\partial_s \boldsymbol{\xi}^\perp, & \boldsymbol{\xi} = \nabla \gamma(\mathbf{p})|_{\mathbf{p}=\mathbf{n}}. \end{cases}$$

When $\gamma(\mathbf{n}) \equiv 1$ (i.e., isotropic surface energy), noting $\mu = \kappa$ and $\mathbf{n} = -\partial_s \mathbf{X}^\perp$, then (1.12b) collapses to $\kappa \mathbf{n} = -\partial_{ss} \mathbf{X}$. In this case, the PFEM is semi-implicit, unconditionally energy-stable, and demonstrates asymptotic equal mesh distribution [5] and thus there is no need to re-mesh during time evolution. Very recently, a structure-preserving PFEM was proposed for the surface diffusion [4]. However, when the PFEM is extended directly to simulate anisotropic surface diffusion, many good properties are lost, especially the unconditional energy stability, except for the Riemannian metric anisotropic surface energy in (1.8) with a modified variational formulation [6]. Recently, by reformulating (1.12b) into a conservative form, an energy-stable PFEM was designed for weakly anisotropic surface diffusion under a very strong condition on $\hat{\gamma}(\theta) = \gamma(-\sin \theta, \cos \theta)$ [22]. To our best knowledge, it is still an open question to design a structure-preserving/energy-stable PFEM for the anisotropic surface diffusion (1.12) with any arbitrary anisotropic surface energy.

The main aim of this paper is to propose a structure-preserving/energy-stable PFEM for the anisotropic surface diffusion (1.12) with arbitrary anisotropic surface energy. We first reformulate (1.12b) into a conservative and self-adjoint form by introducing a novel symmetric positive definite surface energy matrix $Z_k(\mathbf{n})$ depending on the Cahn-Hoffman $\boldsymbol{\xi}$ -vector and a stabilizing function $k(\mathbf{n})$, and then derive a new symmetrized variational formulation for the anisotropic surface diffusion (1.12). The symmetrized variational formulation is first discretized in space by PFEM and then discretized in time by either an implicit structural-preserving scheme (SP-PFEM) which preserves the area in the discretized level or a semi-implicit energy-stable method (ES-PFEM) which needs only solve a linear system at every time step. Under the relatively simple and mild condition on $\gamma(\mathbf{n})$ as

$$(1.13) \quad \gamma(-\mathbf{n}) = \gamma(\mathbf{n}), \quad \forall \mathbf{n} \in \mathbb{S}^1, \quad \gamma(\mathbf{p}) \in C^2(\mathbb{R}^2 \setminus \{\mathbf{0}\}),$$

we show that both SP-PFEM and ES-PFEM are energy dissipative and thus are unconditionally energy stable for almost all anisotropic surface energy $\gamma(\mathbf{n})$ arising in practical applications, including both weakly and strongly anisotropic surface energy. Specifically, for several commonly-used anisotropic surface energies, we construct the stabilizing function $k(\mathbf{n})$ (and thus $Z_k(\mathbf{n})$) explicitly.

The rest of the paper is organized as follows: In section 2, we propose a new symmetrized variational formulation and show its area/mass conservation and energy dissipation. In section 3, we present its semi-discretization in space by PFEM and then full-discretizations by either an implicit structural-preserving method (SP-PFEM) or a semi-implicit energy-stable method (ES-PFEM), and show their properties. In section 4, we prove energy-stability of SP-PFEM and ES-PFEM under the simple and mild condition (1.13) on $\gamma(\mathbf{n})$. Numerical results are reported in section 5 to demonstrate the efficiency in the convergence rate and iteration steps, the energy stability of the proposed symmetrized SP/ES-PFEM, and the area/mass conservation of the symmetrized SP-PFEM, and some conclusions are drawn in section 6.

2. A new symmetrized variational formulation and its properties. In this section, we present a new conservative and self-adjoint formulation of (1.12b) and a new symmetrized variational formulation of (1.12), and prove the area/mass conservation and energy dissipation of the new formulation.

2.1. A symmetric positive definite surface energy matrix. Introducing a symmetric surface energy matrix $Z_k(\mathbf{n})$ as

$$(2.1) \quad Z_k(\mathbf{n}) = \gamma(\mathbf{n})I_2 - \mathbf{n}\boldsymbol{\xi}^T - \boldsymbol{\xi}\mathbf{n}^T + k(\mathbf{n})\mathbf{n}\mathbf{n}^T, \quad \forall \mathbf{n} \in \mathbb{S}^1,$$

where $k(\mathbf{n}) : \mathbb{S}^1 \rightarrow \mathbb{R}^+$ is a stabilizing function to be determined later, then we have

LEMMA 2.1 (symmetric and conservative form). *With the symmetric surface energy matrix $Z_k(\mathbf{n})$ in (2.1), the anisotropic surface diffusion (1.12) can be reformulated as*

$$(2.2a) \quad \begin{cases} \mathbf{n} \cdot \partial_t \mathbf{X} = \partial_{ss} \mu, \\ \mu \mathbf{n} = -\partial_s (Z_k(\mathbf{n}) \partial_s \mathbf{X}). \end{cases}$$

Proof. From (1.3), noting (1.6), we get

$$(2.3) \quad \boldsymbol{\xi}^\perp = \gamma(\mathbf{n})\mathbf{n}^\perp + (\boldsymbol{\xi} \cdot \boldsymbol{\tau})\boldsymbol{\tau}^\perp = \gamma(\mathbf{n})\boldsymbol{\tau} - (\boldsymbol{\xi} \cdot \boldsymbol{\tau})\mathbf{n}.$$

From (2.1), noticing (1.6) and (2.3), and using $\mathbf{n} \cdot \boldsymbol{\tau} = 0$, we get

$$(2.4) \quad \begin{aligned} Z_k(\mathbf{n})\partial_s \mathbf{X} &= Z_k(\mathbf{n})\boldsymbol{\tau} = (\gamma(\mathbf{n})I_2 - \mathbf{n}\boldsymbol{\xi}^T - \boldsymbol{\xi}\mathbf{n}^T + k(\mathbf{n})\mathbf{n}\mathbf{n}^T)\boldsymbol{\tau} \\ &= \gamma(\mathbf{n})\boldsymbol{\tau} - (\boldsymbol{\xi} \cdot \boldsymbol{\tau})\mathbf{n} + (\mathbf{n} \cdot \boldsymbol{\tau})(k(\mathbf{n})\mathbf{n} - \boldsymbol{\xi}) \\ &= \gamma(\mathbf{n})\boldsymbol{\tau} - (\boldsymbol{\xi} \cdot \boldsymbol{\tau})\mathbf{n} \\ &= \boldsymbol{\xi}^\perp. \end{aligned}$$

Plugging (2.4) into (1.12), we obtain (2.2) immediately. \square

REMARK 2.1. *When $\gamma(\mathbf{n}) \equiv 1$ and taking $k(\mathbf{n}) \equiv 2$ in (2.1), we have $\mu = \kappa$ and $\boldsymbol{\xi} = \mathbf{n}$, and thus $Z_k(\mathbf{n}) \equiv I_2$. Then (2.2) collapses to the standard formulation by PFEM for surface diffusion [5]. Similarly, when $\gamma(\mathbf{n})$ is taken as the Riemannian metric anisotropic surface energy (1.8), by taking $k(\mathbf{n}) = \gamma(\mathbf{n})^{-1} \text{Tr}(G)$ with $\text{Tr}(G)$ denoting the trace of G , then (2.2) collapses to the formulation used in [6].*

2.2. The variational formulation. Let $\mathbb{T} = \mathbb{R}/\mathbb{Z} = [0, 1]$ be the periodic unit interval and we parameterize the evolution curves $\Gamma(t)$ as

$$(2.5) \quad \Gamma(t) := \mathbf{X}(\rho, t) = (x(\rho, t), y(\rho, t))^T : \mathbb{T} \times \mathbb{R}^+ \rightarrow \mathbb{R}^2.$$

The arclength parameter s is computed by $s(\rho, t) = \int_0^\rho |\partial_q \mathbf{X}| \, dq$ with its derivative $\partial_\rho s = |\partial_\rho \mathbf{X}|$. By the introduced time independent variable ρ , the evolving curve $\Gamma(t)$ can then be parameterized over a fixed domain $\rho \in \mathbb{T} = [0, 1]$. We do not distinguish the two parameterization $\mathbf{X}(\rho, t)$ and $\mathbf{X}(s, t)$ for $\Gamma(t)$ if there is no ambiguity. For the closed curve $\Gamma(t)$, we also introduce the Sobolev space defined as

$$(2.6) \quad L^2(\mathbb{T}) = \left\{ u : \mathbb{T} \rightarrow \mathbb{R} \mid \int_{\Gamma(t)} |u(s)|^2 ds = \int_{\mathbb{I}} |u(s(\rho, t))|^2 \partial_\rho s \, d\rho < +\infty \right\},$$

equipped with the L^2 -inner product

$$(2.7) \quad (u, v)_{\Gamma(t)} := \int_{\Gamma(t)} u(s)v(s) \, ds = \int_{\mathbb{T}} u(s(\rho, t))v(s(\rho, t))\partial_\rho s \, d\rho, \quad \forall u, v \in L^2(\mathbb{T}),$$

which can be easily extended to $[L^2(\mathbb{T})]^2$. Moreover, we define the Sobolev space

$$(2.8) \quad H^1(\mathbb{T}) := \{u : \mathbb{T} \rightarrow \mathbb{R}, \text{ and } u \in L^2(\mathbb{T}), \partial_\rho u \in L^2(\mathbb{T})\}.$$

Multiplying a test function $\varphi(\rho) \in H^1(\mathbb{T})$ to (2.2a), and then integrating over $\Gamma(t)$ and taking integration by parts, we have

$$(2.9) \quad \left(\mathbf{n} \cdot \partial_t \mathbf{X}, \varphi\right)_{\Gamma(t)} = \left(\partial_{ss}\mu, \varphi\right)_{\Gamma(t)} = -\left(\partial_s \mu, \partial_s \varphi\right)_{\Gamma(t)}.$$

Similarly, by multiplying a test function $\boldsymbol{\omega} = (\omega_1, \omega_2)^T \in [H^1(\mathbb{T})]^2$ to (2.2b), we can then get

$$(2.10) \quad \left(\mu \mathbf{n}, \boldsymbol{\omega}\right)_{\Gamma(t)} = \left(-\partial_s(Z_k(\mathbf{n})\partial_s \mathbf{X}), \boldsymbol{\omega}\right)_{\Gamma(t)} = \left(Z_k(\mathbf{n})\partial_s \mathbf{X}, \partial_s \boldsymbol{\omega}\right)_{\Gamma(t)}.$$

By combining the two weak formulations (2.9) and (2.10), we now get the novel symmetrized variational formulation for the anisotropic surface diffusion (2.2) (or (1.5)) with the initial condition (1.7). More precisely, for a given initial curve $\Gamma_0 := \Gamma(0) = \mathbf{X}(\rho, 0) = \mathbf{X}_0(L_0\rho) \in [H^1(\mathbb{T})]^2$, find the solution $\Gamma(t) := \mathbf{X}(\cdot, t) \in [H^1(\mathbb{T})]^2$ and $\mu(\cdot, t) \in H^1(\mathbb{T})$ such that:

$$(2.11a) \quad \left(\mathbf{n} \cdot \partial_t \mathbf{X}, \varphi\right)_{\Gamma(t)} + \left(\partial_s \mu, \partial_s \varphi\right)_{\Gamma(t)} = 0, \quad \forall \varphi \in H^1(\mathbb{T}),$$

$$(2.11b) \quad \left(\mu, \mathbf{n} \cdot \boldsymbol{\omega}\right)_{\Gamma(t)} - \left(Z_k(\mathbf{n})\partial_s \mathbf{X}, \partial_s \boldsymbol{\omega}\right)_{\Gamma(t)} = 0, \quad \forall \boldsymbol{\omega} \in [H^1(\mathbb{T})]^2.$$

2.3. Area/mass conservation and energy dissipation. Let $A(t)$ denote the area (i.e., the region $\Omega(t)$ enclosed by the curve $\Gamma(t)$) and $W_c(t)$ denote the free energy (or weighted perimeter), which are defined as

$$(2.12) \quad A(t) := \int_{\Omega(t)} 1 \, d\mathbf{x} = \int_0^{L(t)} y(s, t) \partial_s x(s, t) \, ds, \quad W_c(t) := \int_{\Gamma(t)} \gamma(\mathbf{n}) \, ds, \quad t \geq 0.$$

For the above variational problem (2.11), we have

PROPOSITION 2.2 (area/mass conservation and energy dissipation). *Let $(\mathbf{X}(\cdot, t), \mu(\cdot, t)) \in [H^1(\mathbb{T})]^2 \times H^1(\mathbb{T})$ be a solution of the variational problem (2.11), then the area/mass $A(t)$ is conserved and the energy $W_c(t)$ is dissipative, i.e.*

$$(2.13) \quad A(t) \equiv \int_0^{L_0} y_0(s) x'_0(s) \, ds, \quad W_c(t) \leq W_c(t_1) \leq \int_0^{L_0} \gamma(\mathbf{n}) \, ds, \quad t \geq t_1 \geq 0.$$

Proof. The proof of area/mass conservation is similar to the Proposition 2.1 in [22], thus we omit the details for brevity.

To prove the energy dissipation in (2.13), differentiating $W_c(t)$ defined in (2.12) with respect to t , noting (1.3), (2.4), (2.11b) with $\boldsymbol{\omega} = \partial_t \mathbf{X}$, and (2.11a) with $\varphi = \mu$,

and $\partial_t \mathbf{n} = (\boldsymbol{\tau} \cdot \partial_t \mathbf{n}) \boldsymbol{\tau} = -(\mathbf{n} \cdot \partial_s \partial_t \mathbf{X}) \boldsymbol{\tau}$, we have

$$\begin{aligned}
\dot{W}_c(t) &= \frac{d}{dt} \int_0^{L(t)} \gamma(\mathbf{n}) ds = \frac{d}{dt} \int_0^1 \gamma(\mathbf{n}) \partial_\rho s d\rho \\
&= \int_0^1 (\gamma(\mathbf{n}) \partial_t \partial_\rho s + \nabla \gamma(\mathbf{n}) \cdot \partial_t \mathbf{n} \partial_\rho s) d\rho \\
&= \int_0^1 (\gamma(\mathbf{n}) (\boldsymbol{\tau} \cdot \partial_\rho \partial_t \mathbf{X}) + \boldsymbol{\xi} \cdot \partial_t \mathbf{n} \partial_\rho s) d\rho \\
&= \int_0^1 (\gamma(\mathbf{n}) \boldsymbol{\tau} - (\boldsymbol{\xi} \cdot \boldsymbol{\tau}) \mathbf{n}) \cdot \partial_s \partial_t \mathbf{X} \partial_\rho s d\rho \\
(2.14) \quad &= \left(Z_k(\mathbf{n}) \partial_s \mathbf{X}, \partial_s \partial_t \mathbf{X} \right)_{\Gamma(t)} = - \left(\partial_s \mu, \partial_s \mu \right)_{\Gamma(t)} \leq 0, \quad t \geq 0,
\end{aligned}$$

which immediately implies the energy dissipation in (2.13). \square

3. PFEM discretizations and their properties. In this section, we first discretize the variational problem (2.11) in space by PFEM and show its area/mass conservation and energy dissipation. Then we further discretize the semi-discretization in time by either a structure preserving PFEM (SP-PFEM) which conserves area/mass in the discretized level or a semi-implicit energy-stable PFEM (ES-PFEM) with its well-posedness being established.

3.1. A semi-discretization in space by PFEM and its properties. Let $N > 0$ be an integer, the mesh size $h = 1/N$, the grid points $\rho_j = jh$ for $j = 0, 1, \dots, N$, where $\rho_0 = \rho_N$ by periodic, and the subintervals $I_j = [\rho_{j-1}, \rho_j]$ for $j = 1, 2, \dots, N$. Then we can give the uniform partition of the torus \mathbb{T} by $\mathbb{T} = [0, 1] = \bigcup_{j=1}^N I_j$. Moreover, the finite element subspace of $H^1(\mathbb{T})$ is given by

$$\mathbb{K}^h = \mathbb{K}^h(\mathbb{T}) := \{u^h \in C(\mathbb{T}) \mid u^h|_{I_j} \in \mathcal{P}_1, \forall j = 1, 2, \dots, N\},$$

where \mathcal{P}_1 stands for the space of all polynomials which degree is at most 1.

Let the piecewise linear curve $\Gamma^h(t) := \mathbf{X}^h(\cdot, t) = (x^h(\cdot, t), y^h(\cdot, t))^T \in [\mathbb{K}^h]^2$ be the numerical approximation of $\Gamma(t) := \mathbf{X}(\cdot, t) \in [H^1(\mathbb{T})]^2$ and the piecewise linear function $\mu^h(t) \in \mathbb{K}^h$ be the numerical approximation of $\mu(\cdot, t) \in H^1(\mathbb{T})$, where $(\mathbf{X}(\cdot, t), \mu(\cdot, t)) \in [H^1(\mathbb{T})]^2 \times H^1(\mathbb{T})$ is given by the variational problem (2.11). Then $\Gamma^h(t)$ is formed by ordered line segments $\{\mathbf{h}_j(t)\}_{j=1}^N$ and we can assume that $\forall t \geq 0$, the segments $\mathbf{h}_j(t)$ satisfy

$$(3.1) \quad h_{\min}(t) := \min_{1 \leq j \leq N} |\mathbf{h}_j(t)| > 0, \quad \mathbf{h}_j(t) := \mathbf{X}^h(\rho_j, t) - \mathbf{X}^h(\rho_{j-1}, t), \quad 1 \leq j \leq N,$$

where $|\mathbf{h}_j(t)|$ is the length of the line segment $\mathbf{h}_j(t)$ for $j = 1, 2, \dots, N$.

The outward unit normal vector \mathbf{n}^h , the unit tangential vector $\boldsymbol{\tau}^h$, and the Cahn-Hoffman $\boldsymbol{\xi}$ -vector $\boldsymbol{\xi}^h$ of the curve $\Gamma^h(t)$ are constant vectors in the interior of each interval I_j which can be computed by $\mathbf{h}_j(t)$ as

$$(3.2) \quad \mathbf{n}^h|_{I_j} = -\frac{(\mathbf{h}_j)^\perp}{|\mathbf{h}_j|} := \mathbf{n}_j^h, \quad \boldsymbol{\tau}^h|_{I_j} = \frac{\mathbf{h}_j}{|\mathbf{h}_j|} := \boldsymbol{\tau}_j^h, \quad \boldsymbol{\xi}^h|_{I_j} = \boldsymbol{\xi}(\mathbf{n}_j^h) := \boldsymbol{\xi}_j^h.$$

Furthermore, for two scalar or vector functions u and v in \mathbb{K}^h or $[\mathbb{K}^h]^2$ respectively, the mass lumped inner product $(\cdot, \cdot)_{\Gamma^h}^h$ over Γ^h is defined as

$$(3.3) \quad (u, v)_{\Gamma^h}^h := \frac{1}{2} \sum_{j=1}^N |\mathbf{h}_j| \left[(u \cdot v)(\rho_j^-) + (u \cdot v)(\rho_{j-1}^+) \right],$$

where $u(\rho_j^\pm) = \lim_{\rho \rightarrow \rho_j^\pm} u(\rho)$ for $0 \leq j \leq N$.

Suppose $\Gamma^h(0) := \mathbf{X}^h(\rho, 0) \in [\mathbb{K}^h]^2$ is the piecewise linear interpolation of the initial curve $\mathbf{X}_0(s)$ in (1.7), where $\mathbf{X}^h(\rho = \rho_j, 0) = \mathbf{X}_0(s = s_j^0)$ with $s_j^0 = L_0 \rho_j$ for $j = 0, 1, \dots, N$. Then the spatial semi-discretization of the symmetrized variational formulation (2.11) can be stated as: for a given initial curve $\Gamma^h(0) = \mathbf{X}^h(\cdot, 0) \in [\mathbb{K}^h]^2$, find the solution $\Gamma^h(t) := \mathbf{X}^h(\cdot, t) = (x^h(\cdot, t), y^h(\cdot, t))^T \in [\mathbb{K}^h]^2$ and $\mu^h(\cdot, t) \in \mathbb{K}^h$, such that

$$(3.4a) \quad \left(\mathbf{n}^h \cdot \partial_t \mathbf{X}^h, \varphi^h \right)_{\Gamma^h}^h + \left(\partial_s \mu^h, \partial_s \varphi^h \right)_{\Gamma^h}^h = 0, \quad \forall \varphi^h \in \mathbb{K}^h,$$

$$(3.4b) \quad \left(\mu^h, \mathbf{n}^h \cdot \boldsymbol{\omega}^h \right)_{\Gamma^h}^h - \left(Z_k(\mathbf{n}^h) \partial_s \mathbf{X}^h, \partial_s \boldsymbol{\omega}^h \right)_{\Gamma^h}^h = 0, \quad \forall \boldsymbol{\omega}^h \in [\mathbb{K}^h]^2.$$

Let $A^h(t)$ be the area/mass of the interior region of the piecewise linear closed curve $\Gamma^h(t)$, and $W_c^h(t)$ be its energy, which are defined as

$$(3.5) \quad A^h(t) = \frac{1}{2} \sum_{j=1}^N [x_j^h(t) - x_{j-1}^h(t)][y_j^h(t) + y_{j-1}^h(t)], \quad W_c^h(t) = \sum_{j=1}^N |\mathbf{h}_j(t)| \gamma(\mathbf{n}_j^h).$$

For the spatial semi-discretization (3.4), we also have

PROPOSITION 3.1 (area/mass conservation and energy dissipation). *Let $(\mathbf{X}^h(\cdot, t), \mu^h(\cdot, t)) \in [\mathbb{K}^h]^2 \times \mathbb{K}^h$ be a solution of the spatial semi-discretization (3.4), then the area/mass $A^h(t)$ is conserved and the energy $W_c^h(t)$ is dissipative, i.e.*

$$(3.6) \quad A^h(t) \equiv A^h(0) = \frac{1}{2} \sum_{j=1}^N [x_0(s_j) - x_0(s_{j-1})][y_0(s_j) + y_0(s_{j-1})], \quad t \geq 0,$$

$$(3.7) \quad W_c^h(t) \leq W_c^h(t_1) \leq W_c^h(0) = \sum_{j=1}^N |\mathbf{h}_j(0)| \gamma(\mathbf{n}_j^h), \quad t \geq t_1 \geq 0.$$

Proof. The proof of area/mass conservation is similar to the Proposition 3.1 in [22], thus we omit the details for brevity.

To prove the energy dissipation (3.7), noticing $\mathbf{n}_j^h \cdot \mathbf{n}_j^h = 1$ and $\mathbf{n}_j^h \cdot \boldsymbol{\tau}_j^h = 0$, we have

$$(3.8) \quad 2\dot{\mathbf{n}}_j^h \cdot \mathbf{n}_j^h = 0, \quad \dot{\mathbf{n}}_j^h \cdot \boldsymbol{\tau}_j^h + \dot{\boldsymbol{\tau}}_j^h \cdot \mathbf{n}_j^h = 0; \quad 1 \leq j \leq N,$$

which immediately implies

$$(3.9) \quad \dot{\mathbf{n}}_j^h = (\dot{\mathbf{n}}_j^h \cdot \mathbf{n}_j^h) \mathbf{n}_j^h + (\dot{\mathbf{n}}_j^h \cdot \boldsymbol{\tau}_j^h) \boldsymbol{\tau}_j^h = -(\dot{\boldsymbol{\tau}}_j^h \cdot \mathbf{n}_j^h) \boldsymbol{\tau}_j^h = -\frac{\dot{\mathbf{h}}_j \cdot \mathbf{n}_j^h}{|\mathbf{h}_j|} \boldsymbol{\tau}_j^h, \quad 1 \leq j \leq N.$$

Differentiating $W_c^h(t)$ in (3.5) with respect to t , noticing (3.8) and (3.9), we obtain

$$\begin{aligned}
\dot{W}_c^h(t) &= \frac{d}{dt} \left(\sum_{j=1}^N |\mathbf{h}_j(t)| \gamma(\mathbf{n}_j^h) \right) = \sum_{j=1}^N \left(\gamma(\mathbf{n}_j^h) \frac{d}{dt} |\mathbf{h}_j(t)| + \nabla \gamma(\mathbf{n}_j^h) \cdot \dot{\mathbf{n}}_j^h |\mathbf{h}_j(t)| \right) \\
&= \sum_{j=1}^N \left(\gamma(\mathbf{n}_j^h) \boldsymbol{\tau}_j^h \cdot \dot{\mathbf{h}}_j(t) - \nabla \gamma(\mathbf{n}_j^h) \cdot \boldsymbol{\tau}_j^h \mathbf{n}_j^h \cdot \dot{\mathbf{h}}_j(t) \right) \\
(3.10) \quad &= \sum_{j=1}^N |\mathbf{h}_j(t)| \left(\gamma(\mathbf{n}_j^h) \boldsymbol{\tau}_j^h - \nabla \gamma(\mathbf{n}_j^h) \cdot \boldsymbol{\tau}_j^h \mathbf{n}_j^h \right) \cdot \frac{\dot{\mathbf{h}}_j(t)}{|\mathbf{h}_j(t)|}.
\end{aligned}$$

Noting

$$(3.11) \quad \partial_s \mathbf{X}^h \Big|_{I_j} = \frac{\mathbf{h}_j(t)}{|\mathbf{h}_j(t)|}, \quad \partial_s \partial_t \mathbf{X}^h \Big|_{I_j} = \frac{1}{|\mathbf{h}_j(t)|} \partial_t \mathbf{X}^h \Big|_{I_j} = \frac{\dot{\mathbf{h}}_j(t)}{|\mathbf{h}_j(t)|}, \quad 1 \leq j \leq N,$$

and using (3.4b) with $\boldsymbol{\omega}^h = \partial_t \mathbf{X}^h$ and (3.4a) with $\varphi^h = \mu^h$, we get

$$\begin{aligned}
\dot{W}_c^h(t) &= \sum_{j=1}^N |\mathbf{h}_j(t)| \left(Z_k(\mathbf{n}_j^h) \boldsymbol{\tau}_j^h \right) \cdot \frac{\dot{\mathbf{h}}_j(t)}{|\mathbf{h}_j(t)|} \\
&= \sum_{j=1}^N |\mathbf{h}_j(t)| \left(Z_k(\mathbf{n}_j^h) \partial_s \mathbf{X}^h \Big|_{I_j} \right) \cdot \left(\partial_s \partial_t \mathbf{X}^h \Big|_{I_j} \right) \\
&= \left(Z_k(\mathbf{n}_j^h) \partial_s \mathbf{X}^h, \partial_s \partial_t \mathbf{X}^h \right)_{\Gamma^h}^h = \left(\mu^h, \mathbf{n}^h \cdot \partial_t \mathbf{X}^h \right)_{\Gamma^h}^h \\
(3.12) \quad &= - \left(\partial_s \mu^h, \partial_s \mu^h \right)_{\Gamma^h}^h \leq 0, \quad t \geq 0,
\end{aligned}$$

which implies the energy dissipation in (3.7). \square

3.2. A structure-preserving PFEM. Let $\tau > 0$ be the time step size, and $t_m = m\tau$ be the discrete time levels for each $m \geq 0$. Let $\Gamma^m := \mathbf{X}^m(\rho) = (x^m(\rho), y^m(\rho))^T \in [\mathbb{K}^h]^2$ be the numerical approximation of $\Gamma^h(t_m) = \mathbf{X}^h(\rho, t_m) \in [\mathbb{K}^h]^2$ and $\mu^m \in \mathbb{K}^h$ be the numerical approximations of $\mu^h(t_m) \in \mathbb{K}^h$ for each $m \geq 0$, where $(\mathbf{X}^h(\cdot, t), \mu^h(t))$ is the solution of the semi-discretization (3.4). Similarly, Γ^m is formed by the ordered line segments $\{\mathbf{h}_j^m\}_{j=1}^N$ defined by

$$(3.13) \quad \mathbf{h}_j^m := \mathbf{X}^m(\rho_j) - \mathbf{X}^m(\rho_{j-1}), \quad j = 1, 2, \dots, N.$$

Again, for each $m \geq 0$, the outward unit normal vector \mathbf{n}^m , the unit tangential vector $\boldsymbol{\tau}^m$, and the Cahn-Hoffman $\boldsymbol{\xi}$ -vector $\boldsymbol{\xi}^m$ of the curve Γ^m are constant vectors in the interior of each interval I_j which can be computed as

$$(3.14) \quad \mathbf{n}^m \Big|_{I_j} = - \frac{(\mathbf{h}_j^m)^\perp}{|\mathbf{h}_j^m|} := \mathbf{n}_j^m, \quad \boldsymbol{\tau}^m \Big|_{I_j} = \frac{\mathbf{h}_j^m}{|\mathbf{h}_j^m|} := \boldsymbol{\tau}_j^m, \quad \boldsymbol{\xi}^m \Big|_{I_j} = \boldsymbol{\xi}(\mathbf{n}_j^m) := \boldsymbol{\xi}_j^m.$$

Following the idea in [4] to design a structure-preserving PFEM (SP-PFEM) for surface diffusion, i.e., using the backward Euler method in time and the information of the curve at current time step and next time step to linearly interpolate the normal vector, a symmetrized structure-preserving PFEM (SP-PFEM) discretization of (3.4)

is given as: for a given initial curve $\Gamma^0 := \Gamma^h(0) \in [\mathbb{K}^h]^2$, for $m \geq 0$, find the curve $\Gamma^{m+1} := \mathbf{X}^{m+1}(\cdot) \in [\mathbb{K}^h]^2$ and the chemical potential $\mu^{m+1}(\cdot) \in \mathbb{K}^h$, such that

$$(3.15a) \quad \left(\frac{\mathbf{X}^{m+1} - \mathbf{X}^m}{\tau} \cdot \mathbf{n}^{m+\frac{1}{2}}, \varphi^h \right)_{\Gamma^m}^h + \left(\partial_s \mu^{m+1}, \partial_s \varphi^h \right)_{\Gamma^m}^h = 0, \quad \forall \varphi^h \in \mathbb{K}^h,$$

$$(3.15b) \quad \left(\mu^{m+1}, \mathbf{n}^{m+\frac{1}{2}} \cdot \boldsymbol{\omega}^h \right)_{\Gamma^m}^h - \left(Z_k(\mathbf{n}^m) \partial_s \mathbf{X}^{m+1}, \partial_s \boldsymbol{\omega}^h \right)_{\Gamma^m}^h = 0, \quad \forall \boldsymbol{\omega}^h \in [\mathbb{K}^h]^2,$$

where s is the arclength parameter of Γ^m and $\mathbf{n}^{m+\frac{1}{2}}$ is defined as

$$(3.16) \quad \mathbf{n}^{m+\frac{1}{2}} := -\frac{1}{2} (\partial_s \mathbf{X}^m + \partial_s \mathbf{X}^{m+1})^\perp = -\frac{1}{2} \frac{1}{|\partial_\rho \mathbf{X}^m|} (\partial_\rho \mathbf{X}^m + \partial_\rho \mathbf{X}^{m+1})^\perp,$$

and for any scalar or vector function $f \in \mathbb{K}^h([\mathbb{K}^h]^2)$ respectively, we compute its derivative with respect to the arclength parameter on Γ^m as $\partial_s f = |\partial_\rho \mathbf{X}^m|^{-1} \partial_\rho f$.

The above scheme is ‘‘weakly implicit’’ with only one nonlinear term introduced in (3.15a) and (3.15b), respectively. In particular, the nonlinear term is a polynomial function of degree at most two with respect to the components of \mathbf{X}^{m+1} and μ^{m+1} . Again, similar to [4] for surface diffusion, the fully-implicit SP-PFEM (3.15) can be efficiently and accurately solved by the Newton’s iterative method in practical computations.

Let A^m be the area/mass of the interior region of the piecewise linear closed curve Γ^m , and W_c^m ($m \geq 0$) be its energy, which are defined as

$$(3.17) \quad A^m := \frac{1}{2} \sum_{j=1}^N [x_j^m - x_{j-1}^m][y_j^m + y_{j-1}^m], \quad W_c^m := W_c(\Gamma^m) = \sum_{j=1}^N |\mathbf{h}_j^m| \gamma(\mathbf{n}_j^m).$$

Similar to the proof in [4, Theorem 2.1] for surface diffusion, we can also prove the following area/mass conservation and the details are omitted here for brevity.

THEOREM 3.2 (area/mass conservation). *Let $(\mathbf{X}^m(\cdot), \mu^m(\cdot)) \in [\mathbb{K}^h]^2 \times \mathbb{K}^h$ be a solution of the SP-PFEM (3.15), then the area/mass A^m in (3.17) is conserved, i.e.*

$$(3.18) \quad A^m \equiv A^0 = \frac{1}{2} \sum_{j=1}^N [x_j^0 - x_{j-1}^0][y_j^0 + y_{j-1}^0], \quad m \geq 0.$$

3.3. A semi-implicit energy-stable PFEM. In practical computations, if one does not want to solve a nonlinear coupled system at every time step, we also propose the following semi-implicit symmetrized energy-stable PFEM (ES-PFEM) discretization of (3.4) : for a given $\Gamma^0 := \Gamma^h(0) \in [\mathbb{K}^h]^2$, for $m \geq 0$, find the closed curve $\Gamma^{m+1} := \mathbf{X}^{m+1}(\cdot) = (x^{m+1}(\cdot), y^{m+1}(\cdot))^T \in [\mathbb{K}^h]^2$ and a chemical potential $\mu^{m+1}(\cdot) \in \mathbb{K}^h$, such that

$$(3.19a) \quad \left(\frac{\mathbf{X}^{m+1} - \mathbf{X}^m}{\tau} \cdot \mathbf{n}^m, \varphi^h \right)_{\Gamma^m}^h + \left(\partial_s \mu^{m+1}, \partial_s \varphi^h \right)_{\Gamma^m}^h = 0, \quad \forall \varphi^h \in \mathbb{K}^h,$$

$$(3.19b) \quad \left(\mu^{m+1}, \mathbf{n}^m \cdot \boldsymbol{\omega}^h \right)_{\Gamma^m}^h - \left(Z_k(\mathbf{n}^m) \partial_s \mathbf{X}^{m+1}, \partial_s \boldsymbol{\omega}^h \right)_{\Gamma^m}^h = 0, \quad \forall \boldsymbol{\omega}^h \in [\mathbb{K}^h]^2.$$

REMARK 3.1. *Similar to the Theorem 4.1 in [22], we can prove the well-posedness result of the symmetrized ES-PFEM (3.19) under the same assumptions in [22, Theorem 4.1]. The only difference is here we use the positive definiteness of $Z_k(\mathbf{n})$ instead of the $G(\theta)$ in [22].*

4. Energy dissipation. In this section, we show energy dissipation of the SP-PFEM (3.15) and ES-PFEM (3.19) under the simple and mild condition (1.13) on the anisotropic surface energy $\gamma(\mathbf{n})$ when $k(\mathbf{n})$ in (2.1) is chosen properly.

4.1. Choice of the stabilizing function. In order to ensure $Z_k(\mathbf{n})$ to be positive definite, since $\text{Tr}(Z_k(\mathbf{n})) = k(\mathbf{n})$, we need request $k(\mathbf{n}) > 0$ for $\mathbf{n} \in \mathbb{S}^1$. Denote

$$(4.1) \quad F(\mathbf{n}, \hat{\mathbf{n}}) = \frac{\gamma(\hat{\mathbf{n}})^2 - \gamma(\mathbf{n})^2 + 2\gamma(\mathbf{n})(\boldsymbol{\xi} \cdot \hat{\mathbf{n}}^\perp)(\mathbf{n} \cdot \hat{\mathbf{n}}^\perp)}{\gamma(\mathbf{n})(\mathbf{n} \cdot \hat{\mathbf{n}}^\perp)^2}, \quad \forall \mathbf{n} \neq \pm \hat{\mathbf{n}} \in \mathbb{S}^1.$$

THEOREM 4.1 (existence of limit). *Under the condition (1.13) on the anisotropic surface energy $\gamma(\mathbf{n})$, we have*

$$(4.2) \quad \lim_{\substack{\hat{\mathbf{n}} \rightarrow \mathbf{n} \\ \hat{\mathbf{n}} \in \mathbb{S}^1}} F(\mathbf{n}, \hat{\mathbf{n}}) = (\mathbf{n}^\perp)^T H_\gamma(\mathbf{n}) \mathbf{n}^\perp + \frac{|\boldsymbol{\xi}|^2}{\gamma(\mathbf{n})}, \quad \forall \mathbf{n} \in \mathbb{S}^1.$$

Proof. Plugging the vector decomposition $\gamma(\mathbf{n}) = \boldsymbol{\xi} \cdot \mathbf{n} = (\boldsymbol{\xi} \cdot \hat{\mathbf{n}}^\perp)(\mathbf{n} \cdot \hat{\mathbf{n}}^\perp) + (\boldsymbol{\xi} \cdot \hat{\mathbf{n}})(\mathbf{n} \cdot \hat{\mathbf{n}})$ and $1 = \mathbf{n} \cdot \mathbf{n} = (\mathbf{n} \cdot \hat{\mathbf{n}}^\perp)^2 + (\mathbf{n} \cdot \hat{\mathbf{n}})^2$ into (4.1), we get

$$(4.3) \quad \begin{aligned} F(\mathbf{n}, \hat{\mathbf{n}}) &= \frac{\gamma(\hat{\mathbf{n}})^2 - \gamma(\mathbf{n})^2 + 2\gamma(\mathbf{n})^2 - 2\gamma(\mathbf{n})(\boldsymbol{\xi} \cdot \hat{\mathbf{n}})(\mathbf{n} \cdot \hat{\mathbf{n}})}{\gamma(\mathbf{n})|\mathbf{n} - \hat{\mathbf{n}}|^2(1 - |\mathbf{n} - \hat{\mathbf{n}}|^2/4)} \\ &= \frac{\gamma(\hat{\mathbf{n}})^2 + \gamma(\mathbf{n})^2 - 2\gamma(\mathbf{n})(\boldsymbol{\xi} \cdot \hat{\mathbf{n}})(1 - |\mathbf{n} - \hat{\mathbf{n}}|^2/2)}{\gamma(\mathbf{n})|\mathbf{n} - \hat{\mathbf{n}}|^2(1 - |\mathbf{n} - \hat{\mathbf{n}}|^2/4)} \\ &= \frac{1}{1 - |\mathbf{n} - \hat{\mathbf{n}}|^2/4} \left[\frac{\gamma(\hat{\mathbf{n}})^2 - \gamma(\mathbf{n})^2 - 2\gamma(\mathbf{n})(\boldsymbol{\xi} \cdot (\hat{\mathbf{n}} - \mathbf{n}))}{\gamma(\mathbf{n})|\mathbf{n} - \hat{\mathbf{n}}|^2} + \boldsymbol{\xi} \cdot \hat{\mathbf{n}} \right]. \end{aligned}$$

Here we use the following equality

$$\mathbf{n} \cdot \hat{\mathbf{n}}^\perp = \frac{|\mathbf{n}|^2 + |\hat{\mathbf{n}}|^2 - |\mathbf{n} - \hat{\mathbf{n}}|^2}{2} = 1 - \frac{|\mathbf{n} - \hat{\mathbf{n}}|^2}{2}.$$

Under the condition (1.13) on the anisotropic surface energy $\gamma(\mathbf{n})$, using Taylor expansion and noting $\nabla \gamma(\mathbf{p})^2 = 2\gamma(\mathbf{p})\nabla \gamma(\mathbf{p})$ and $\boldsymbol{\xi} = \nabla \gamma(\mathbf{p})|_{\mathbf{p}=\mathbf{n}}$, we obtain

$$\gamma(\mathbf{p})^2 - \gamma(\mathbf{n})^2 = 2\gamma(\mathbf{n})\boldsymbol{\xi} \cdot (\mathbf{p} - \mathbf{n}) + (\mathbf{p} - \mathbf{n})^T \left[\gamma(\mathbf{n})H_\gamma(\mathbf{n}) + \boldsymbol{\xi}\boldsymbol{\xi}^T \right] (\mathbf{p} - \mathbf{n}) + o(|\mathbf{p} - \mathbf{n}|^2),$$

which immediately implies for $\mathbf{n} \in \mathbb{S}^1$

$$(4.4) \quad \lim_{\substack{\mathbf{p} \rightarrow \mathbf{n} \\ \mathbf{p} \in \mathbb{S}^1}} \frac{\gamma(\mathbf{p})^2 - \gamma(\mathbf{n})^2 - 2\gamma(\mathbf{n})\boldsymbol{\xi} \cdot (\mathbf{p} - \mathbf{n})}{|\mathbf{n} - \mathbf{p}|^2} = \gamma(\mathbf{n}) (\mathbf{n}^\perp)^T H_\gamma(\mathbf{n}) \mathbf{n}^\perp + (\boldsymbol{\xi} \cdot \mathbf{n}^\perp)^2.$$

Combining (4.3) and (4.4), noting (1.3) to get $\gamma(\mathbf{n}) = \boldsymbol{\xi} \cdot \mathbf{n}$, we obtain

$$(4.5) \quad \begin{aligned} \lim_{\substack{\hat{\mathbf{n}} \rightarrow \mathbf{n} \\ \hat{\mathbf{n}} \in \mathbb{S}^1}} F(\mathbf{n}, \hat{\mathbf{n}}) &= \frac{1}{\gamma(\mathbf{n})} \lim_{\substack{\mathbf{p} \rightarrow \mathbf{n} \\ \mathbf{p} \in \mathbb{S}^1}} \frac{\gamma(\mathbf{p})^2 - \gamma(\mathbf{n})^2 - 2\gamma(\mathbf{n})\boldsymbol{\xi} \cdot (\mathbf{p} - \mathbf{n})}{|\mathbf{n} - \mathbf{p}|^2} + \boldsymbol{\xi} \cdot \mathbf{n} \\ &= (\mathbf{n}^\perp)^T H_\gamma(\mathbf{n}) \mathbf{n}^\perp + \frac{(\boldsymbol{\xi} \cdot \mathbf{n}^\perp)^2}{\gamma(\mathbf{n})} + \boldsymbol{\xi} \cdot \mathbf{n} \\ &= (\mathbf{n}^\perp)^T H_\gamma(\mathbf{n}) \mathbf{n}^\perp + \frac{(\boldsymbol{\xi} \cdot \mathbf{n}^\perp)^2 + \gamma(\mathbf{n}) \boldsymbol{\xi} \cdot \mathbf{n}}{\gamma(\mathbf{n})} \\ &= (\mathbf{n}^\perp)^T H_\gamma(\mathbf{n}) \mathbf{n}^\perp + \frac{(\boldsymbol{\xi} \cdot \mathbf{n}^\perp)^2 + (\boldsymbol{\xi} \cdot \mathbf{n})^2}{\gamma(\mathbf{n})} \\ &= (\mathbf{n}^\perp)^T H_\gamma(\mathbf{n}) \mathbf{n}^\perp + \frac{|\boldsymbol{\xi}|^2}{\gamma(\mathbf{n})}. \end{aligned}$$

The proof is completed. \square

Under the condition (1.13), for any $\mathbf{n} \in \mathbb{S}^1$, it is easy to see that $F(\mathbf{n}, \hat{\mathbf{n}})$ is a continuous function for $\hat{\mathbf{n}} \in \mathbb{S}^1$ with $\hat{\mathbf{n}} \neq -\mathbf{n}$. This, together with the above Theorem, suggests us to define the following minimal stabilizing function $k_0(\mathbf{n}) : \mathbb{S}^1 \rightarrow \mathbb{R}^+$ as

$$(4.6) \quad k_0(\mathbf{n}) := \max_{\hat{\mathbf{n}} \in \mathbb{S}_n^1} F(\mathbf{n}, \hat{\mathbf{n}}), \quad \text{with } \mathbb{S}_n^1 := \{\hat{\mathbf{n}} \in \mathbb{S}^1 \mid \hat{\mathbf{n}} \cdot \mathbf{n} \geq 0\}, \quad \mathbf{n} \in \mathbb{S}^1.$$

THEOREM 4.2 (existence of stabilizing function). *Under the condition (1.13) on $\gamma(\mathbf{n})$ and assume $k(\mathbf{n}) \geq k_0(\mathbf{n})$ for $\mathbf{n} \in \mathbb{S}^1$ in (2.1), we have*

$$(4.7) \quad \gamma(\mathbf{n})[(\hat{\mathbf{n}}^\perp)^T Z_k(\mathbf{n}) \hat{\mathbf{n}}^\perp] \geq \gamma(\hat{\mathbf{n}})^2, \quad \forall \mathbf{n}, \hat{\mathbf{n}} \in \mathbb{S}^1.$$

In addition, we have an alternative definition of $k_0(\mathbf{n})$ in (4.6) as

$$(4.8) \quad k_0(\mathbf{n}) = \inf \left\{ k(\mathbf{n}) \mid \gamma(\mathbf{n})[(\hat{\mathbf{n}}^\perp)^T Z_k(\mathbf{n}) \hat{\mathbf{n}}^\perp] \geq \gamma(\hat{\mathbf{n}})^2, \quad \forall \hat{\mathbf{n}} \in \mathbb{S}^1 \right\}, \quad \mathbf{n} \in \mathbb{S}^1.$$

Proof. Assume $k(\mathbf{n}) \geq k_0(\mathbf{n})$ for $\mathbf{n} \in \mathbb{S}^1$. For any $\mathbf{n} \in \mathbb{S}^1$, when $\hat{\mathbf{n}} \in \mathbb{S}_n^1$, i.e. $\hat{\mathbf{n}} \cdot \mathbf{n} \geq 0$, plugging (2.1) into the left hand of (4.7), noting (4.1) and (4.6), we have

$$(4.9) \quad \begin{aligned} \gamma(\mathbf{n})[(\hat{\mathbf{n}}^\perp)^T Z_k(\mathbf{n}) \hat{\mathbf{n}}^\perp] &= \gamma(\mathbf{n})^2 - 2\gamma(\mathbf{n})(\boldsymbol{\xi} \cdot \hat{\mathbf{n}}^\perp)(\mathbf{n} \cdot \hat{\mathbf{n}}^\perp) + \gamma(\mathbf{n})k(\mathbf{n})(\mathbf{n} \cdot \hat{\mathbf{n}}^\perp)^2 \\ &\geq \gamma(\mathbf{n})^2 - 2\gamma(\mathbf{n})(\boldsymbol{\xi} \cdot \hat{\mathbf{n}}^\perp)(\mathbf{n} \cdot \hat{\mathbf{n}}^\perp) + \gamma(\mathbf{n})k_0(\mathbf{n})(\mathbf{n} \cdot \hat{\mathbf{n}}^\perp)^2 \\ &\geq \gamma(\mathbf{n})^2 - 2\gamma(\mathbf{n})(\boldsymbol{\xi} \cdot \hat{\mathbf{n}}^\perp)(\mathbf{n} \cdot \hat{\mathbf{n}}^\perp) + \gamma(\mathbf{n})F(\mathbf{n}, \hat{\mathbf{n}})(\mathbf{n} \cdot \hat{\mathbf{n}}^\perp)^2 \\ &= \gamma(\hat{\mathbf{n}})^2. \end{aligned}$$

On the other hand, when $\hat{\mathbf{n}} \cdot \mathbf{n} < 0$, then $-\hat{\mathbf{n}} \cdot \mathbf{n} > 0$, from (4.9) by replacing $\hat{\mathbf{n}}$ by $-\hat{\mathbf{n}}$ and noting $\gamma(-\hat{\mathbf{n}}) = \gamma(\hat{\mathbf{n}})$, we have

$$(4.10) \quad \gamma(\mathbf{n})[(\hat{\mathbf{n}}^\perp)^T Z_k(\mathbf{n}) \hat{\mathbf{n}}^\perp] = \gamma(\mathbf{n})[(-\hat{\mathbf{n}}^\perp)^T Z_k(\mathbf{n}) (-\hat{\mathbf{n}}^\perp)] \geq \gamma(-\hat{\mathbf{n}})^2 = \gamma(\hat{\mathbf{n}})^2.$$

Combining (4.9) and (4.10), we get (4.7) immediately.

From the above proof, it is easy to see that

$$\gamma(\mathbf{n})[(\hat{\mathbf{n}}^\perp)^T Z_{k_0}(\mathbf{n}) \hat{\mathbf{n}}^\perp] \geq \gamma(\hat{\mathbf{n}})^2, \quad \forall \mathbf{n}, \hat{\mathbf{n}} \in \mathbb{S}^1,$$

which immediately implies

$$(4.11) \quad k_0(\mathbf{n}) \geq \inf \left\{ k(\mathbf{n}) \mid \gamma(\mathbf{n})[(\hat{\mathbf{n}}^\perp)^T Z_k(\mathbf{n}) \hat{\mathbf{n}}^\perp] \geq \gamma(\hat{\mathbf{n}})^2, \quad \forall \hat{\mathbf{n}} \in \mathbb{S}^1 \right\}, \quad \forall \mathbf{n} \in \mathbb{S}^1.$$

On the other hand, suppose $Z_k(\mathbf{n})$ satisfies (4.7), then we have

$$(4.12) \quad \gamma(\mathbf{n}) \left(\gamma(\mathbf{n}) - 2(\boldsymbol{\xi} \cdot \hat{\mathbf{n}}^\perp)(\mathbf{n} \cdot \hat{\mathbf{n}}^\perp) + k(\mathbf{n})(\mathbf{n} \cdot \hat{\mathbf{n}}^\perp)^2 \right) \geq \gamma(\hat{\mathbf{n}})^2, \quad \forall \hat{\mathbf{n}} \in \mathbb{S}_n^1,$$

which implies

$$(4.13) \quad k(\mathbf{n}) \geq \frac{\gamma(\hat{\mathbf{n}})^2 - \gamma(\mathbf{n})^2 + 2\gamma(\mathbf{n})(\boldsymbol{\xi} \cdot \hat{\mathbf{n}}^\perp)(\mathbf{n} \cdot \hat{\mathbf{n}}^\perp)}{\gamma(\mathbf{n})(\mathbf{n} \cdot \hat{\mathbf{n}}^\perp)^2} = F(\mathbf{n}, \hat{\mathbf{n}}), \quad \forall \hat{\mathbf{n}} \in \mathbb{S}_n^1.$$

By condition (1.13), this inequality holds for all $\hat{\mathbf{n}} \in \mathbb{S}^1$. Thus we get $k(\mathbf{n}) \geq k_0(\mathbf{n})$, which implies

$$(4.14) \quad k_0(\mathbf{n}) \leq \inf \left\{ k(\mathbf{n}) \mid \gamma(\mathbf{n})[(\hat{\mathbf{n}}^\perp)^T Z_k(\mathbf{n}) \hat{\mathbf{n}}^\perp] \geq \gamma(\hat{\mathbf{n}})^2, \quad \forall \hat{\mathbf{n}} \in \mathbb{S}^1 \right\}, \quad \forall \mathbf{n} \in \mathbb{S}^1.$$

Combining (4.11) and (4.14), we obtain (4.8) immediately. \square

COROLLARY 4.3 (positivity of the minimal stabilizing function). *Assume (4.7) is satisfied, then $Z_k(\mathbf{n})$ is a symmetric positive definite matrix and*

$$(4.15) \quad \gamma(-\mathbf{n}) = \gamma(\mathbf{n}), \quad k_0(\mathbf{n}) > 0, \quad \forall \mathbf{n} \in \mathbb{S}^1.$$

Proof. Taking $\hat{\mathbf{n}} = -\mathbf{n}$ in (4.7), noting the first equality in (4.9), we get $\gamma(\mathbf{n})^2 \geq \gamma(-\mathbf{n})^2$ which suggests $\gamma(-\mathbf{n})^2 \geq \gamma(-(-\mathbf{n}))^2 = \gamma(\mathbf{n})^2$, and thus we obtain the first equality in (4.15) since $\gamma(\mathbf{n}) > 0$. From (4.7), we get $Z_k(\mathbf{n})$ is symmetric positive definite, which implies $k(\mathbf{n}) = \text{Tr}(Z_k(\mathbf{n})) \geq k_0(\mathbf{n}) = \text{Tr}(Z_{k_0}(\mathbf{n})) > 0$ for $\mathbf{n} \in \mathbb{S}^1$. \square

If we consider from the anisotropic surface energy $\gamma(\mathbf{n})$ to its corresponding minimal stabilizing function $k_0(\mathbf{n})$ defined in (4.8) (or (4.6)) as a mapping, then it is a sub-linear mapping, i.e. positive homogeneity and subadditivity.

LEMMA 4.4 (positive homogeneity and subadditivity). *Assume $k_0(\mathbf{n})$, $k_1(\mathbf{n})$ and $k_2(\mathbf{n})$ be the minimal stabilizing functions for the anisotropic surface energies $\gamma(\mathbf{n})$, $\gamma_1(\mathbf{n})$ and $\gamma_2(\mathbf{n})$, respectively, then we have*

- (i) if $\gamma_1(\mathbf{n}) = c\gamma(\mathbf{n})$ with $c > 0$, then $k_1(\mathbf{n}) = ck_0(\mathbf{n})$ for $\mathbf{n} \in \mathbb{S}^1$, and
- (ii) if $\gamma(\mathbf{n}) = \gamma_1(\mathbf{n}) + \gamma_2(\mathbf{n})$, then $k_0(\mathbf{n}) \leq k_1(\mathbf{n}) + k_2(\mathbf{n})$ for $\mathbf{n} \in \mathbb{S}^1$.

Proof. From (1.3), we get

$$(4.16) \quad \boldsymbol{\xi} = \nabla\gamma(\mathbf{p})|_{\mathbf{p}=\mathbf{n}}, \quad \boldsymbol{\xi}_1 = \nabla\gamma_1(\mathbf{p})|_{\mathbf{p}=\mathbf{n}}, \quad \boldsymbol{\xi}_2 = \nabla\gamma_2(\mathbf{p})|_{\mathbf{p}=\mathbf{n}}.$$

(i) If $\gamma_1(\mathbf{n}) = c\gamma(\mathbf{n})$, we get $\boldsymbol{\xi}_1 = c\boldsymbol{\xi}$. This, together with (4.1), implies

$$(4.17) \quad F_1(\mathbf{n}, \hat{\mathbf{n}}) = \frac{\gamma_1(\hat{\mathbf{n}})^2 - \gamma_1(\mathbf{n})^2 + 2\gamma_1(\mathbf{n})(\boldsymbol{\xi}_1 \cdot \hat{\mathbf{n}}^\perp)(\mathbf{n} \cdot \hat{\mathbf{n}}^\perp)}{\gamma_1(\mathbf{n})(\mathbf{n} \cdot \hat{\mathbf{n}}^\perp)^2} = cF(\mathbf{n}, \hat{\mathbf{n}}).$$

Combining (4.17) and (4.6), we obtain the positive homogeneity immediately.

(ii) If $\gamma(\mathbf{n}) = \gamma_1(\mathbf{n}) + \gamma_2(\mathbf{n})$, we have

$$\begin{aligned} Z_{k_1+k_2}(\mathbf{n}) &= \gamma(\mathbf{n})I - \nabla\gamma(\mathbf{n})\mathbf{n}^T - \mathbf{n}(\nabla\gamma(\mathbf{n}))^T + (k_1(\mathbf{n}) + k_2(\mathbf{n}))\mathbf{n}\mathbf{n}^T \\ &= Z_{k_1}^{(1)}(\mathbf{n}) + Z_{k_2}^{(2)}(\mathbf{n}), \end{aligned}$$

where

$$\begin{aligned} Z_{k_1}^{(1)}(\mathbf{n}) &= \gamma_1(\mathbf{n})I - \nabla\gamma_1(\mathbf{n})\mathbf{n}^T - \mathbf{n}(\nabla\gamma_1(\mathbf{n}))^T + k_1(\mathbf{n})\mathbf{n}\mathbf{n}^T, \\ Z_{k_2}^{(2)}(\mathbf{n}) &= \gamma_2(\mathbf{n})I - \nabla\gamma_2(\mathbf{n})\mathbf{n}^T - \mathbf{n}(\nabla\gamma_2(\mathbf{n}))^T + k_2(\mathbf{n})\mathbf{n}\mathbf{n}^T. \end{aligned}$$

By using Cauchy inequality, we get

$$\begin{aligned} &\gamma(\mathbf{n})[(\hat{\mathbf{n}}^\perp)^T Z_{k_1+k_2}(\mathbf{n})\hat{\mathbf{n}}^\perp] \\ &= (\gamma_1(\mathbf{n}) + \gamma_2(\mathbf{n}))[(\hat{\mathbf{n}}^\perp)^T Z_{k_1}^{(1)}(\mathbf{n})\hat{\mathbf{n}}^\perp + (\hat{\mathbf{n}}^\perp)^T Z_{k_2}^{(2)}(\mathbf{n})\hat{\mathbf{n}}^\perp] \\ &\geq \left(\sqrt{\gamma_1(\mathbf{n})[(\hat{\mathbf{n}}^\perp)^T Z_{k_1}^{(1)}(\mathbf{n})\hat{\mathbf{n}}^\perp]} + \sqrt{\gamma_2(\mathbf{n})[(\hat{\mathbf{n}}^\perp)^T Z_{k_2}^{(2)}(\mathbf{n})\hat{\mathbf{n}}^\perp]} \right)^2 \\ (4.18) \quad &\geq (\gamma_1(\hat{\mathbf{n}}) + \gamma_2(\hat{\mathbf{n}}))^2 = \gamma(\hat{\mathbf{n}})^2. \end{aligned}$$

Combining (4.18) and (4.8), we get $k_0(\mathbf{n}) \leq k_1(\mathbf{n}) + k_2(\mathbf{n})$ for $\mathbf{n} \in \mathbb{S}^1$. \square

4.2. Energy dissipation. For the SP-PFEM (3.15) and the ES-PFEM (3.19), we have the following theorem:

THEOREM 4.5 (energy dissipation). *Assume the surface energy matrix $Z_k(\mathbf{n})$ satisfies (4.7), then both SP-PFEM (3.15) and ES-PFEM (3.19) are unconditionally energy stable, i.e. for any $\tau > 0$, we have*

$$(4.19) \quad W_c^{m+1} \leq W_c^m \leq \dots \leq W_c^0 = \sum_{j=1}^N |\mathbf{h}_j^0| \gamma(\mathbf{n}_j^0), \quad \forall m \geq 0.$$

Proof. Under (4.7), we know that $Z_k(\mathbf{n})$ is symmetric positive definite. Thus we have

$$(4.20) \quad \left(Z_k(\mathbf{n})\mathbf{u}, \mathbf{u} - \mathbf{v} \right) \geq \frac{1}{2} \left(Z_k(\mathbf{n})\mathbf{u}, \mathbf{u} \right) - \frac{1}{2} \left(Z_k(\mathbf{n})\mathbf{v}, \mathbf{v} \right), \quad \forall \mathbf{u}, \mathbf{v} \in \mathbb{R}^2.$$

Using (2.4) and $\boldsymbol{\xi} \cdot \mathbf{n} = \gamma(\mathbf{n})$, we get

$$(4.21) \quad (\partial_s \mathbf{X}^m)^T Z_k(\mathbf{n}^m) \partial_s \mathbf{X}^m = \boldsymbol{\tau}^m \cdot (\boldsymbol{\xi}^m)^\perp = \gamma(\mathbf{n}^m).$$

Combining (4.21) and (4.20), noting $Z_k(\mathbf{n})$ satisfies (4.7), we obtain

$$\begin{aligned} & \left(Z_k(\mathbf{n}^m) \partial_s \mathbf{X}^{m+1}, \partial_s \mathbf{X}^{m+1} - \partial_s \mathbf{X}^m \right)_{\Gamma^m}^h + \int_{\Gamma^m} \gamma(\mathbf{n}^m) ds \\ & \geq \frac{1}{2} \left(Z_k(\mathbf{n}^m) \partial_s \mathbf{X}^{m+1}, \partial_s \mathbf{X}^{m+1} \right)_{\Gamma^m}^h + \frac{1}{2} \int_{\Gamma^m} \gamma(\mathbf{n}^m) ds \\ & = \sum_{j=1}^N \frac{(\mathbf{h}_j^{m+1})^T Z_k(\mathbf{n}_j^m) \mathbf{h}_j^{m+1} + \gamma(\mathbf{n}_j^m) |\mathbf{h}_j^m|^2}{2|\mathbf{h}_j^m|} \\ & \geq \sum_{j=1}^N |\mathbf{h}_j^{m+1}| \sqrt{\left(\mathbf{n}_j^{m+1} \right)^\perp{}^T Z_k(\mathbf{n}_j^m) \mathbf{n}_j^{m+1} \perp} \gamma(\mathbf{n}_j^m) \\ (4.22) \quad & \geq \sum_{j=1}^N |\mathbf{h}_j^{m+1}| \sqrt{\frac{\gamma^2(\mathbf{n}_j^{m+1})}{\gamma(\mathbf{n}_j^m)}} \gamma(\mathbf{n}_j^m) = \sum_{j=1}^N |\mathbf{h}_j^{m+1}| \gamma(\mathbf{n}_j^{m+1}) = \int_{\Gamma^{m+1}} \gamma(\mathbf{n}^{m+1}) ds. \end{aligned}$$

Taking $\varphi^h = \mu^{m+1}$ in (3.15a) and $\boldsymbol{\omega}^h = \mathbf{X}^{m+1} - \mathbf{X}^m$ in (3.15b) and combining the inequality (4.22), we get

$$\begin{aligned} W_c^{m+1} - W_c^m &= \int_{\Gamma^{m+1}} \gamma(\mathbf{n}^{m+1}) ds - \int_{\Gamma^m} \gamma(\mathbf{n}^m) ds \\ &\leq \left(Z_k(\mathbf{n}^m) \partial_s \mathbf{X}^{m+1}, \partial_s \mathbf{X}^{m+1} - \partial_s \mathbf{X}^m \right)_{\Gamma^m}^h \\ &= \left(\mu^{m+1}, \mathbf{n}^{m+\frac{1}{2}} \cdot (\mathbf{X}^{m+1} - \mathbf{X}^m) \right)_{\Gamma^m}^h \\ (4.23) \quad &= -\tau \left(\partial_s \mu^{m+1}, \partial_s \mu^{m+1} \right)_{\Gamma^m}^h \leq 0, \quad \forall m \geq 0, \end{aligned}$$

which immediately implies the energy dissipation (4.19) for the SP-PFEM (3.15). The proof for the ES-PFEM (3.19) is similar and thus the details are omitted here for brevity. \square

Combining Theorems 4.2 and 4.5, we have

COROLLARY 4.6 (energy dissipation). *Assume $\gamma(\mathbf{n})$ satisfies (1.13) and taking $k(\mathbf{n}) \geq k_0(\mathbf{n})$ in (2.1), then both SP-PFEM (3.15) and ES-PFEM (3.19) are unconditionally energy stable.*

4.3. Explicit formulas for the minimal stabilizing function. Here we give explicit formulas of the minimal stabilizing function $k_0(\mathbf{n})$ for several popular anisotropic surface energies $\gamma(\mathbf{n})$ in applications. Denote

$$J = \begin{pmatrix} 0 & -1 \\ 1 & 0 \end{pmatrix}, \quad Z_0(\mathbf{n}) = \begin{pmatrix} 1 & n_1 n_2 \\ n_1 n_2 & 1 \end{pmatrix}, \quad \forall \mathbf{n} = \begin{pmatrix} n_1 \\ n_2 \end{pmatrix} \in \mathbb{S}^1.$$

LEMMA 4.7 (Riemannian metric). *When $\gamma(\mathbf{n})$ is taken as the Riemannian metric anisotropic surface energy (1.8), we have*

$$(4.24) \quad k_0(\mathbf{n}) = \gamma(\mathbf{n})^{-1} \text{Tr}(G), \quad Z_{k_0}(\mathbf{n}) = \gamma(\mathbf{n})^{-1} J^T G J, \quad \forall \mathbf{n} \in \mathbb{S}^1.$$

Proof. A direct computation shows

$$\gamma(\mathbf{n}) (\hat{\mathbf{n}}^\perp)^T Z_{k_0}(\mathbf{n}) \hat{\mathbf{n}}^\perp - \gamma(\hat{\mathbf{n}})^2 = (J \hat{\mathbf{n}}^\perp)^T G (J \hat{\mathbf{n}}^\perp) - \gamma(\hat{\mathbf{n}})^2 = 0, \quad \forall \mathbf{n}, \hat{\mathbf{n}} \in \mathbb{S}^1.$$

By Theorem 4.2, we get $k_0(\mathbf{n}) \leq \gamma(\mathbf{n})^{-1} \text{Tr}(G)$. On the other hand, taking the limit $\hat{\mathbf{n}} \rightarrow \mathbf{n}$ in (4.6), after a direct calculation, we find $k_0(\mathbf{n}) \geq \gamma(\mathbf{n})^{-1} \text{Tr}(G)$. Thus we obtain (4.24) and $Z_{k_0}(\mathbf{n}) = Z(\mathbf{n}) = \gamma(\mathbf{n})^{-1} J^T G J$. \square

LEMMA 4.8 (l^r -norm metric). *When $\gamma(\mathbf{n})$ is taken as the l^r -norm metric anisotropic surface energy (1.9), we have*

- (i) when $r = 4$, $k_0(\mathbf{n}) = 2\gamma(\mathbf{n})^{-3}$ and $Z_{k_0}(\mathbf{n}) = \gamma(\mathbf{n})^{-3} Z_0(\mathbf{n})$, and
- (ii) when $r = 6$, $k_0(\mathbf{n}) = 2\gamma(\mathbf{n})^{-5} (n_1^4 + n_1^2 n_2^2 + n_2^4)$.

Proof. (i) When $r = 4$, a direct computation shows

$$\begin{aligned} \gamma(\mathbf{n}) (\hat{\mathbf{n}}^\perp)^T Z_{k_0}(\mathbf{n}) \hat{\mathbf{n}}^\perp - \gamma(\hat{\mathbf{n}})^2 &= \gamma(\mathbf{n})^{-2} (\hat{\mathbf{n}}^\perp)^T Z_0(\mathbf{n}) \hat{\mathbf{n}}^\perp - \sqrt{\hat{n}_1^4 + \hat{n}_2^4} \\ &= \frac{1 - 2n_1 n_2 \hat{n}_1 \hat{n}_2}{\sqrt{n_1^4 + n_2^4}} - \sqrt{\hat{n}_1^4 + \hat{n}_2^4} \\ &\geq \frac{2 - 4n_1 n_2 \hat{n}_1 \hat{n}_2 - n_1^4 - n_2^4 - \hat{n}_1^4 - \hat{n}_2^4}{2\sqrt{n_1^4 + n_2^4}} \\ &= \frac{(n_1 n_2 - \hat{n}_1 \hat{n}_2)^2}{\sqrt{n_1^4 + n_2^4}} \geq 0, \quad \forall \mathbf{n}, \hat{\mathbf{n}} \in \mathbb{S}^1. \end{aligned}$$

By Theorem 4.2, we get $k_0(\mathbf{n}) \leq 2\gamma(\mathbf{n})^{-3}$. On the other hand, taking $\hat{\mathbf{n}} = (n_2, n_1)^T \in \mathbb{S}^1$ in (4.6), after a direct calculation, we find $k_0(\mathbf{n}) \geq 2\gamma(\mathbf{n})^{-3}$. Thus the conclusions are true.

(ii) When $r = 6$, the proof is similar and its details are omitted here for brevity.

\square

LEMMA 4.9 (2-fold). *When $\gamma(\mathbf{n})$ is taken as the m -fold anisotropy (1.10) with $m = 2$, $\theta_0 = 0$ and $\beta \geq 0$, we have*

$$(4.25) \quad k_0(\mathbf{n}) \leq 4 - 2\gamma(\mathbf{n}) + \frac{4\beta^2}{1-\beta} := k_1(\mathbf{n}),$$

$$(4.26) \quad Z_{k_1}(\mathbf{n}) = (1-\beta) \begin{pmatrix} \frac{\beta+1}{1-\beta} (1 + \frac{2\beta}{1-\beta} n_1^2) & \frac{4\beta^2}{(1-\beta)^2} n_1 n_2 \\ \frac{4\beta^2}{(1-\beta)^2} n_1 n_2 & 1 + \frac{2\beta(3\beta-1)}{(1-\beta)^2} n_2^2 \end{pmatrix}.$$

Proof. A direct computation shows

$$\begin{aligned} & \gamma(\mathbf{n})[(\hat{\mathbf{n}}^\perp)^T Z_{k_1}(\mathbf{n})\hat{\mathbf{n}}^\perp] - \gamma(\hat{\mathbf{n}})^2 \\ &= 4\beta^2 \left(\frac{2\beta}{1-\beta} n_2^2 + (n_1\hat{n}_1 - n_2\hat{n}_2)^2 \right) (n_1\hat{n}_2 - \hat{n}_1 n_2)^2 \\ &\geq 0, \quad \forall \mathbf{n}, \hat{\mathbf{n}} \in \mathbb{S}^1. \end{aligned}$$

By Theorem 4.2, we have $k_0(\mathbf{n}) \leq k_1(\mathbf{n}) = 4 - 2\gamma(\mathbf{n}) + \frac{4\beta^2}{1-\beta}$. \square

5. Numerical results. In this section, we implement the two proposed symmetrized PFEMs (3.15) and (3.19) for the evolution of the closed curves numerically. Numerical results demonstrate some good performances of the proposed schemes, such as the spatial/temporal convergence rates, energy dissipation, area/mass conservation, and asymptotic quasi-equal mesh distribution. Here the manifold distance $M(\Gamma_1, \Gamma_2)$ is used to calculate the difference between two curves Γ_1 and Γ_2 . Suppose Ω_1 and Ω_2 are the inner regions enclosed by the simple closed curves Γ_1 and Γ_2 , respectively. The area of the symmetric difference of Ω_1 and Ω_2 defines the manifold distance $M(\Gamma_1, \Gamma_2)$ [40]:

$$(5.1) \quad M(\Gamma_1, \Gamma_2) := |(\Omega_1 \setminus \Omega_2) \cup (\Omega_2 \setminus \Omega_1)| = |\Omega_1| + |\Omega_2| - 2|\Omega_1 \cap \Omega_2|,$$

where $|\Omega|$ denotes the area of Ω . Since formally the schemes are first-order accurate in time and second-order accurate in space, the mesh size h and the time step τ are chosen as $\tau = \mathcal{O}(h^2)$, e.g. $\tau = h^2$, except where noted. Let $\Gamma^{h,m}$ be the numerical approximation of $\Gamma^h(t = t_m = m\tau)$ with mesh size h and time step τ , then the numerical error is defined as

$$(5.2) \quad e^h(t_m) := M(\Gamma^{h,m}, \Gamma(t = t_m)), \quad m \geq 0.$$

Since in practical computations, the exact solution is not accessible. Here $\Gamma(t = t_m)$ is obtained numerically by using a very fine mesh size $h = h_e$ and a very small time step $\tau = \tau_e$, e.g. $h_e = 2^{-8}$ and $\tau_e = 2^{-16}$.

The normalized area/mass loss $\Delta A^h(t_m)$, and the mesh ratio $R^h(t_m)$, which is used to indicate the mesh quality of the numerical solution Γ^m , are defined as

$$(5.3) \quad \frac{\Delta A^h(t_m)}{A^h(0)} := \frac{A^h(t = t_m) - A^h(0)}{A^h(0)}, \quad R^h(t = t_m) := \frac{\max_{1 \leq j \leq N} |\mathbf{h}_j^m|}{\min_{1 \leq j \leq N} |\mathbf{h}_j^m|}, \quad m \geq 0,$$

where $A^h(t_m)$ is the area/mass of the inner region enclosed by $\Gamma^{h,m}$.

In the following simulations, the initial shape in (1.7) is always taken as an ellipse with length 4 and width 1, and the tolerance of the Newton iteration in SP-PFEM (3.15) is chosen as 10^{-12} .

5.1. Convergence rates and energy dissipation. In order to test spatial convergence rates and properties of the SP-PFEM (3.15), we consider the following different anisotropic surface energies:

- Case I. the Riemannian metric anisotropic surface energy (1.8) with $G = \text{diag}(1, 2)$ which is weakly anisotropic and the corresponding minimal stabilizing function $k_0(\mathbf{n})$ is given explicitly in (4.24);
- Case II. the m -fold anisotropic surface energy (1.10) with $m = 2$, $\theta_0 = 0$ and $\beta = \frac{1}{4}$ which is weakly anisotropic and the corresponding minimal stabilizing function $k_0(\mathbf{n})$ can only be approximately given in (4.25);

- Case III. the m -fold anisotropic surface energy (1.10) with $m = 2$, $\theta_0 = 0$ and $\beta = \frac{1}{2}$ which is strongly anisotropic and the corresponding minimal stabilizing function $k_0(\mathbf{n})$ can only be approximately given in (4.25); and
- Case IV. the l^r -norm metric anisotropic surface energy (1.9) with $r = 4$ which is strongly anisotropic and the corresponding minimal stabilizing function $k_0(\mathbf{n})$ is given explicitly in Lemma 4.8.

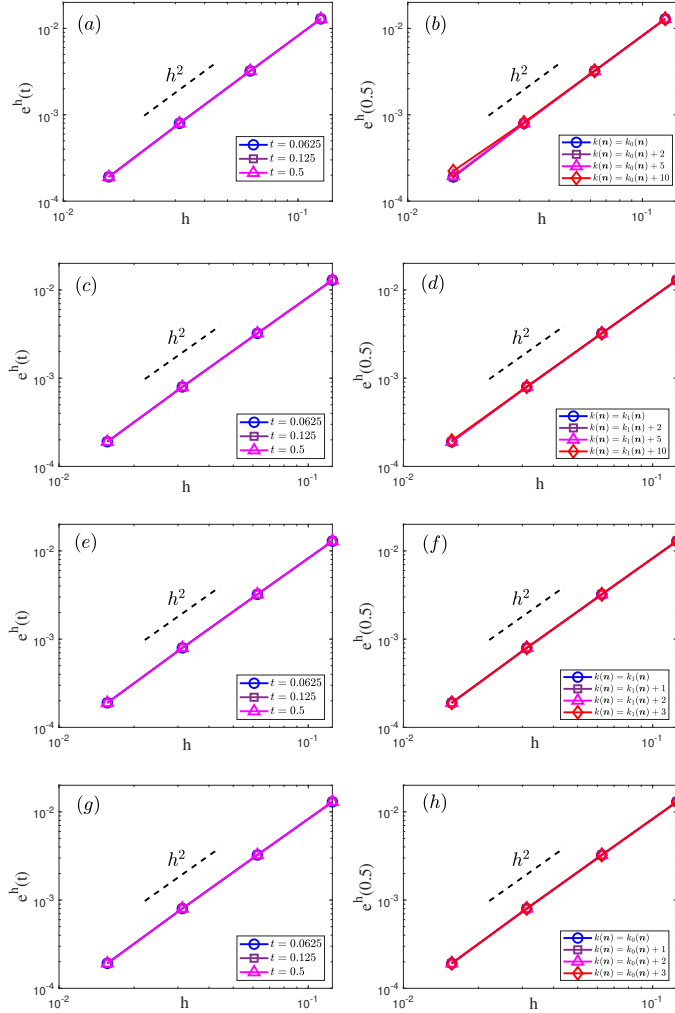


FIG. 5.1. Spatial convergence rates of the SP-PFEM (3.15) for: Case I at different times with $k(\mathbf{n}) = k_0(\mathbf{n})$ in (4.24) (a), and at $t = 0.5$ for different $k(\mathbf{n})$ (b); Case II at different times with $k(\mathbf{n}) = k_1(\mathbf{n})$ in (4.25) (c), and at $t = 0.5$ for different $k(\mathbf{n})$ (d); Case III at different times with $k(\mathbf{n}) = k_1(\mathbf{n})$ in (4.25) (e), and at $t = 0.5$ for different $k(\mathbf{n})$ (f); and Case IV at different times with $k(\mathbf{n}) = k_0(\mathbf{n})$ in Lemma 4.8 (g), and at $t = 0.5$ for different $k(\mathbf{n})$ (h).

Fig. 5.1 plots spatial convergence rates at different times for a fixed choice of $k(\mathbf{n})$ in (2.1) and different choices of $k(\mathbf{n})$ at a fixed time. Fig. 5.2 depicts time evolution of the normalized area/mass loss $\frac{\Delta A^h(t_m)}{A^h(0)}$ for a fixed choice of $k(\mathbf{n})$ in (2.1) and mesh

size h , and the normalized energy $\frac{W_c^h(t_m)}{W_c^h(0)}$ for different mesh sizes h and $k(\mathbf{n})$. Fig. 5.3 shows time evolution of the mesh ratio $R^h(t)$ for different mesh size h , time step τ and $k(\mathbf{n})$.

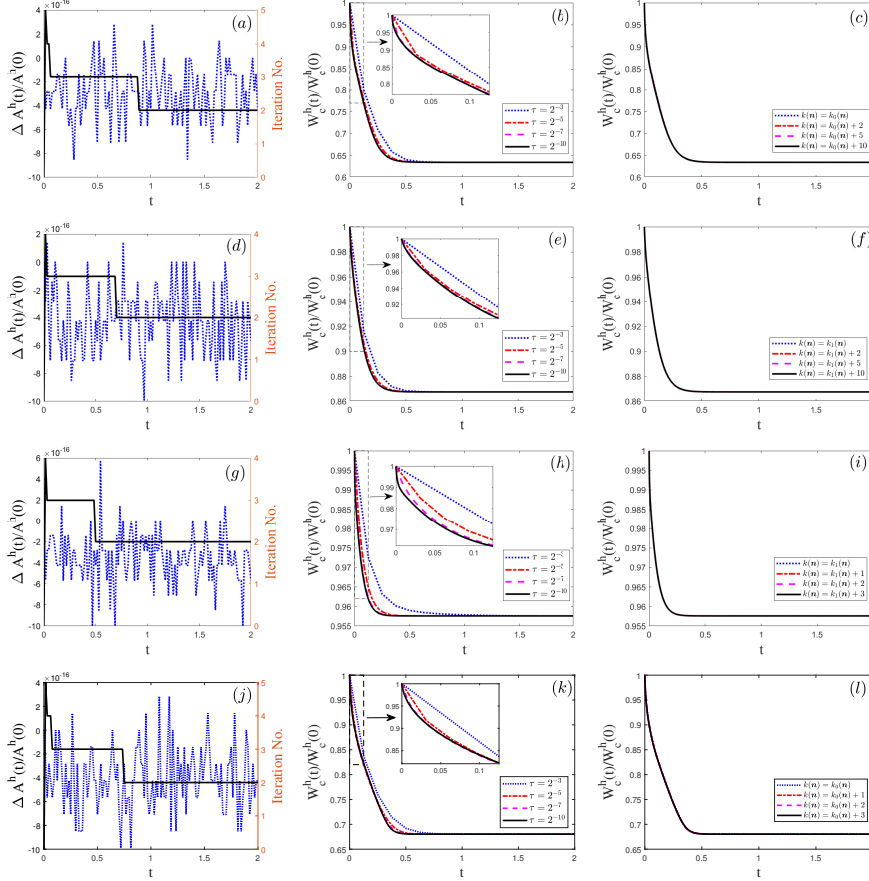


FIG. 5.2. Time evolution of the normalized area/mass loss $\frac{\Delta A^h(t)}{A^h(0)}$ (left column, blue dashed line) and iteration number (left column, black line) and the normalized energy $\frac{W_c^h(t)}{W_c^h(0)}$ (middle and right columns) for: Case I with $k(\mathbf{n}) = k_0(\mathbf{n})$ in (4.24) for $h = 2^{-3}$ (a) and different h (b), and with $h = 2^{-3}$ for different $k(\mathbf{n})$ (c); Case II with $k(\mathbf{n}) = k_1(\mathbf{n})$ in (4.25) for $h = 2^{-3}$ (d) and different h (e), and with $h = 2^{-3}$ for different $k(\mathbf{n})$ (f); Case III with $k(\mathbf{n}) = k_1(\mathbf{n})$ in (4.25) for $h = 2^{-3}$ (g) and different h (h), and with $h = 2^{-3}$ for different $k(\mathbf{n})$ (i); and Case IV with $k(\mathbf{n}) = k_0(\mathbf{n})$ in Lemma 4.8 for $h = 2^{-3}$ (j) and different h (k), and with $h = 2^{-3}$ for different $k(\mathbf{n})$ (l).

From Figs. 5.1–5.3, we can draw the following conclusions for the symmetrized SP-PFEM (3.15) for the evolution of closed curves under anisotropic surface diffusion:

- (i) The symmetrized SP-PFEM (3.15) is second-order accurate in space (cf. Fig. 5.1);
- (ii) The area/mass is conserved numerically up to the round-off error around 10^{-16} (cf. Fig. 5.2(a));
- (iii) The number of Newton iteration at each time step is around 2 to 4, thus it is efficient (cf. Fig. 5.2(a));
- (iv) The scheme is unconditionally energy-stable when the anisotropic surface

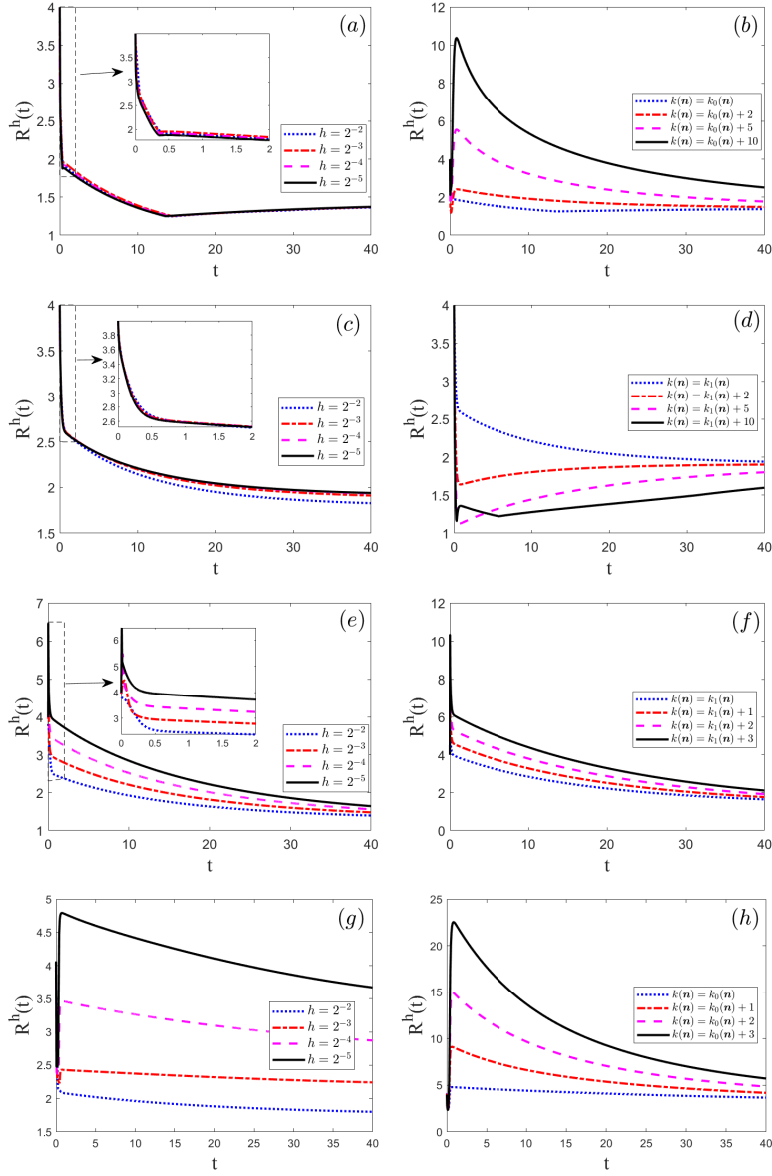


FIG. 5.3. Time evolution of the mesh ratio $R^h(t)$ for: Case I with $k(\mathbf{n}) = k_0(\mathbf{n})$ in (4.24) for different h (a), and with $h = 2^{-5}$ for different $k(\mathbf{n})$ (b); Case II with $k(\mathbf{n}) = k_1(\mathbf{n})$ in (4.25) for different h (c), and with $h = 2^{-5}$ for different $k(\mathbf{n})$ (d); Case III with $k(\mathbf{n}) = k_1(\mathbf{n})$ in (4.25) for different h (e), and with $h = 2^{-5}$ for different $k(\mathbf{n})$ (f); and Case IV with $k(\mathbf{n}) = k_0(\mathbf{n})$ in Lemma 4.8 for different h (g), and with $h = 2^{-5}$ for different $k(\mathbf{n})$ (h).

energy $\gamma(\mathbf{n})$ with $k(\mathbf{n})$ satisfies the energy dissipation condition in Theorem 4.5 (cf. Fig. 5.2(b),(c));

(v) The mesh ratio $R^h(t = t_m)$ will approach a constant C when $t \gg 1$ for each case, which indicates asymptotic quasi-equal mesh distribution. From Fig. 5.3(e)-(h), we can conclude that when the anisotropic surface energy is strong, the stabilizing

function $k(\mathbf{n})$ can not be arbitrarily large, otherwise the mesh ratio will also be very large. Comparing with Fig. 5.3(a)-(d), we observe that for weakly anisotropic surface energies, the stabilizing function k can also affect the asymptotic mesh ratio $\lim_{t \rightarrow \infty} R^h(t)$, but the impact is far smaller than strongly anisotropic surface energies. This indicates that we do not need to compute the minimal stabilizing function $k_0(\mathbf{n})$ accurately for weakly anisotropic surface energies.

The numerical results on spatial convergence rates, energy dissipation and mesh ratio for the ES-PFEM (3.19) are quite similar to those for the SP-PFEM (3.15) and thus they are omitted here for brevity, except the area conservation. Fig. 5.4 depicts time evolution of the normalized area/mass loss $\frac{\Delta A^h(t_m)}{A^h(0)}$ and normalized energy $\frac{W_c^h(t)}{W_c^h(0)}$ for Case IV with different mesh size h and fixed $k(\mathbf{n}) = k_0(\mathbf{n})$ in (2.1).

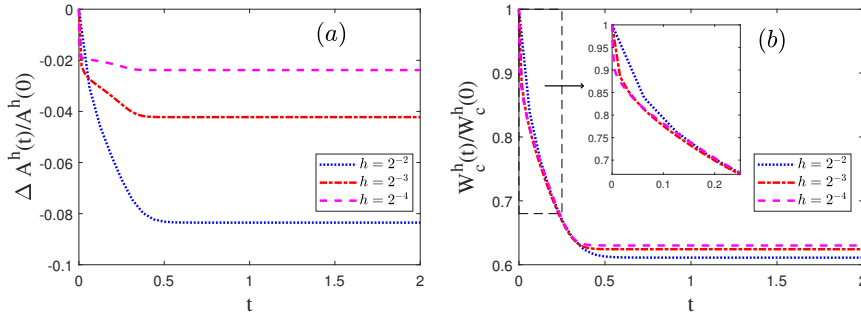


FIG. 5.4. Time evolution of the normalized area/mass loss $\frac{\Delta A^h(t)}{A^h(0)}$ (a) and normalized energy $\frac{W_c^h(t)}{W_c^h(0)}$ (b) for Case IV with $k(\mathbf{n}) = k_0(\mathbf{n})$ in Lemma 4.8 for different h .

Similar conclusions can be drawn for the ES-PFEM (3.19) except that the area/mass is no longer conserved in the discretized level. Based on our numerical results, the area/mass loss is observed numerically at $O(h^2) + O(\tau)$.

5.2. Application for morphological evolutions. Here we apply the SP-PFEM (3.15) to illustrate the morphological evolution under different anisotropic surface energies, i.e., morphological evolutions of closed curves from a 4×1 rectangle towards their corresponding equilibrium shapes. Fig. 5.5 depicts morphological evolutions with $h = 2^{-6}$ and $\tau = h^2$ for the four different weakly anisotropic surface energies including (i) the Riemannian metric (1.8) with $G = \text{diag}(1, 2)$ with $k(\mathbf{n}) = k_0(\mathbf{n})$ given in (4.24), (ii) 2-fold anisotropic energy (1.10) with $m = 2$, $\theta_0 = 0$ and $\beta = \frac{1}{4}$ and $k(\mathbf{n}) = k_1(\mathbf{n})$ given in (4.25), (iii) the l^4 -norm metric (1.9) with $r = 4$ with $k(\mathbf{n}) = k_0(\mathbf{n})$ given in Lemma 4.8, and (iv) the regularized l^1 -norm metric (1.11) with $\varepsilon = 0.1$ by taking $k(\mathbf{n}) = \frac{1.01}{\sqrt{n_1^2 + 0.01n_2^2}} + \frac{1.01}{\sqrt{0.01n_1^2 + n_2^2}}$. Figs. 5.6 and 5.7 show morphological evolutions under the 4-fold $\gamma(\mathbf{n}) = 1 + \frac{3}{10} \cos(4\theta)$ and the 2-fold $\gamma(\mathbf{n}) = 1 + \frac{3}{5} \cos(2(\theta - \frac{\pi}{4}))$, respectively, which are both strongly anisotropic surface energies.

As shown in Fig. 5.5(a)–(b), if we choose the anisotropy as the regularized l^1 -norm metric or the l^4 -norm metric, the equilibrium shapes are almost “faceting” squares; for 2-fold anisotropy (c.f. 5.5(c)), the number of edges in its equilibrium shape is exactly two; And for the Riemannian metric anisotropic energy (c.f. 5.5(d)), the equilibrium shape is an ellipse. The numerical results are perfectly consistent with

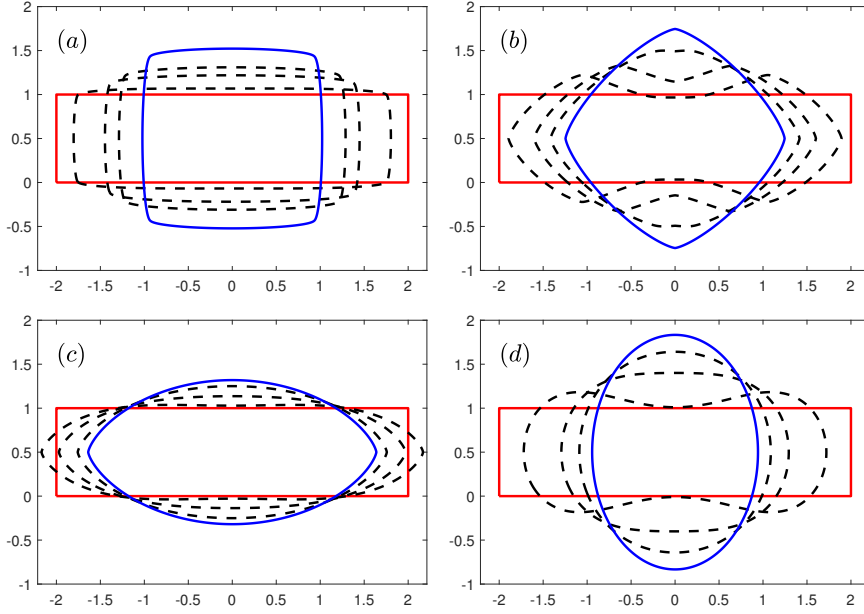


FIG. 5.5. Morphological evolutions of a close rectangular curve under anisotropic surface diffusion with different anisotropic surface energies: (a) regularized l^1 -norm metric; (b) l^4 -norm metric; (c) 2-fold; and (d) Riemannian metric, where the parameters $h = 2^{-6}$, $\tau = h^2$, and the red line, black dashed line and blue line represent the initial shape, intermediate shape and equilibrium shape, respectively.

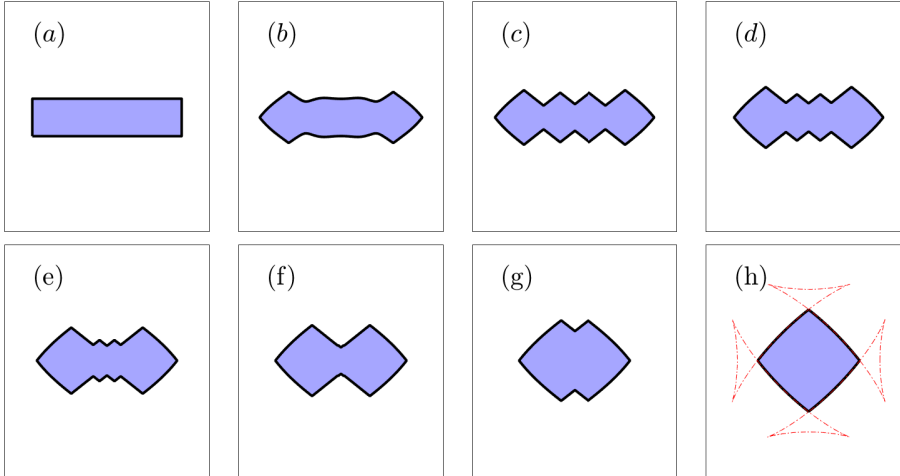


FIG. 5.6. Morphological evolutions of a close rectangular curve under anisotropic surface diffusion with the strongly 4-fold anisotropic surface energy $\gamma(\mathbf{n}) = 1 + \frac{3}{10} \cos(4\theta)$ towards its equilibrium at different times: (a) $t = 0$; (b) $t = 10\tau$; (c) $t = 20\tau$; (d) $t = 160\tau$; (e) $t = 300\tau$; (f) $t = 500\tau$; (g) $t = 1000\tau$; and (h) $t = 5000\tau$, where the parameters are chosen as $h = 2^{-5}$, $\tau = h^2$, and the red dashed line in (h) is the Wulff envelope.

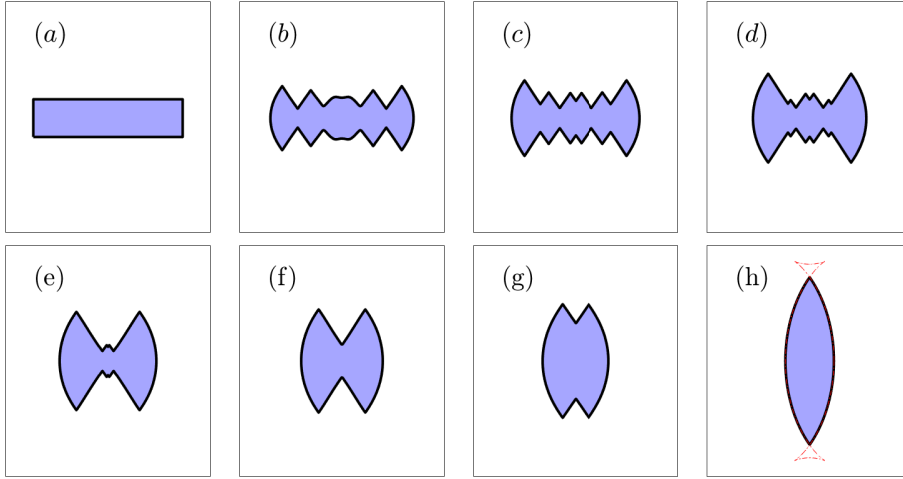


FIG. 5.7. Morphological evolutions of a close rectangular curve under anisotropic surface diffusion with the strongly 2-fold anisotropic surface energy $\gamma(\mathbf{n}) = 1 + \frac{3}{5} \cos(2(\theta - \frac{\pi}{4}))$ towards its equilibrium at different times: (a) $t = 0$; (b) $t = 10\tau$; (c) $t = 60\tau$; (d) $t = 160\tau$; (e) $t = 300\tau$; (f) $t = 500\tau$; (g) $t = 700\tau$; and (h) $t = 5000\tau$, where the parameters are chosen as $h = 2^{-5}$, $\tau = h^2$, and the red dashed line in (h) is the Wulff envelope.

the theoretical predictions by the well-known Wulff construction [35, 6, 2]. Because the surface diffusion is area preserving during the evolution, we can easily obtain its theoretical equilibrium shape (or Wulff shape) by using the expression in [2, 19]. As shown in Figs. 5.6-5.7(h), the numerical equilibrium shapes are again perfectly consistent with the theoretical predictions by the Wulff construction in the strongly anisotropic cases. Furthermore, we can also observe that the numerical equilibrium shape has several ‘‘cusps’’, and these cusps result from the self intersection of the Wulff envelope [2].

6. Conclusions. By utilizing a symmetric positive definite surface energy matrix $Z_k(\mathbf{n})$ and a stabilizing function $k(\mathbf{n})$, we reformulated the anisotropic surface diffusion equation with any arbitrary anisotropic surface energy $\gamma(\mathbf{n})$ into a novel symmetrized form and derived a new variational formulation. We discretized the variational problem in space by the parametric finite element method (PFEM). For temporal discretization, we proposed two different methods: one is a fully implicit structure-preserving time integrator (SP-PFEM), which can rigorously preserve the total area/mass up to machine precision; the other is a semi-implicit energy-stable time integrator (ES-PFEM), which needs only to solve a system of linear equations at each time step and thus it is very efficient. Under a very mild condition on the surface energy $\gamma(\mathbf{n})$, we can rigorously prove that the proposed two numerical schemes are both unconditionally energy-stable. Finally, ample numerical results demonstrated that the two schemes are second-order accurate in space, unconditionally energy-stable, and enjoy very good mesh quality during the evolution. An important contribution is that the new schemes can not only work well for the weakly anisotropic surface energy cases, but also for the strongly anisotropic cases (shown in Figs. 5.6-5.7). In the existing literature, a Willmore regularization energy term is often added into the model to deal with the strongly anisotropic cases [14, 3, 19], but here we only use one unified scheme to tackle the two cases. In the future, we will further

explore the high performance of the schemes, especially for the strongly anisotropic cases; and extend the new variational formulation to anisotropic surface diffusion of open/closed surfaces in three dimensions [21, 39].

Appendix A. The Cahn-Hoffman $\boldsymbol{\xi}$ -vector for several anisotropic surface energies

For the Riemannian metric anisotropic surface energy (1.8), we have

$$(A.1) \quad \gamma(\mathbf{p}) = \sqrt{\mathbf{p}^T G \mathbf{p}}, \quad \forall \mathbf{p} \in \mathbb{R}_*^2 := \mathbb{R}^2 \setminus \{\mathbf{0}\},$$

$$(A.2) \quad \boldsymbol{\xi} = \boldsymbol{\xi}(\mathbf{n}) = \gamma(\mathbf{n})^{-1} G \mathbf{n}, \quad \lambda(\mathbf{n}) = \gamma(\mathbf{n})^{-3} \det(G) > 0, \quad \forall \mathbf{n} \in \mathbb{S}^1.$$

Similarly, for the l^r -norm ($r \geq 2$) metric anisotropic surface energy (1.9), we have

$$(A.3) \quad \gamma(\mathbf{p}) = \|\mathbf{p}\|_{l^r} = (|p_1|^r + |p_2|^r)^{\frac{1}{r}}, \quad \forall \mathbf{p} = (p_1, p_2)^T \in \mathbb{R}_*^2,$$

$$(A.4) \quad \boldsymbol{\xi} = \boldsymbol{\xi}(\mathbf{n}) = \gamma(\mathbf{n})^{1-r} \begin{pmatrix} |n_1|^{r-2} n_1 \\ |n_2|^{r-2} n_2 \end{pmatrix}, \quad \lambda(\mathbf{n}) = (r-1) \frac{|n_1 n_2|^{r-2}}{\gamma(\mathbf{n})^{2r-1}}, \quad \forall \mathbf{n} \in \mathbb{S}^1.$$

Similarly, for the m -fold anisotropic surface energy (1.10) with $\theta_0 = 0$, noting (1.2), we have

$$(A.5) \quad \gamma(\mathbf{p}) = (p_1^2 + p_2^2)^{\frac{1}{2}} (1 + \beta \cos(m\theta)), \quad \forall \mathbf{p} = (p_1, p_2)^T = |p|(-\sin \theta, \cos \theta)^T \in \mathbb{R}_*^2,$$

Plugging (A.5) into (1.3), we get

$$(A.6) \quad \boldsymbol{\xi} = \boldsymbol{\xi}(\mathbf{n}) = \mathbf{n} + \beta \cos(m\theta) \mathbf{n} + \beta m \sin(m\theta) \mathbf{n}^\perp, \quad \forall \mathbf{n} = (-\sin \theta, \cos \theta) \in \mathbb{S}^1,$$

$$(A.7) \quad \lambda(\mathbf{n}) = 1 - \beta(m^2 - 1) \cos(m\theta).$$

Similarly, for the regularized l^1 -norm metric anisotropic surface energy (1.11), we get

$$(A.8) \quad \gamma(\mathbf{p}) = \sqrt{p_1^2 + \varepsilon^2 p_2^2} + \sqrt{\varepsilon^2 p_1^2 + p_2^2}, \quad \forall \mathbf{p} = (p_1, p_2)^T \in \mathbb{R}_*^2,$$

$$(A.9) \quad \boldsymbol{\xi}(\mathbf{n}) = \begin{pmatrix} (D_1(\mathbf{n}) + \varepsilon^2 D_2(\mathbf{n})) n_1 \\ (\varepsilon^2 D_1(\mathbf{n}) + D_2(\mathbf{n})) n_2 \end{pmatrix}, \quad \lambda(\mathbf{n}) = \varepsilon^2 [D_1(\mathbf{n})^3 + D_2(\mathbf{n})^3], \quad \forall \mathbf{n} \in \mathbb{S}^1.$$

where

$$(A.10) \quad D_1(\mathbf{n}) = \frac{1}{\sqrt{n_1^2 + \varepsilon^2 n_2^2}}, \quad D_2(\mathbf{n}) = \frac{1}{\sqrt{\varepsilon^2 n_1^2 + n_2^2}}, \quad \forall \mathbf{n} = (n_1, n_2)^T \in \mathbb{S}^1.$$

For the above different anisotropic energies $\gamma(\mathbf{n})$, their Hessian matrices have the following formulation:

$$(A.11) \quad H_\gamma(\mathbf{n}) = \lambda(\mathbf{n}) \begin{pmatrix} n_2^2 & -n_1 n_2 \\ -n_1 n_2 & n_1^2 \end{pmatrix}, \quad \forall \mathbf{n} = (n_1, n_2)^T \in \mathbb{S}^1.$$

REFERENCES

- [1] E. BÄNSCH, P. MORIN, AND R. H. NOCHETTO, *Surface diffusion of graphs: variational formulation, error analysis, and simulation*, SIAM J. Numer. Anal., 42 (2004), pp. 773–799.
- [2] W. BAO, W. JIANG, D. J. SROLOVITZ, AND Y. WANG, *Stable equilibria of anisotropic particles on substrates: a generalized winterbottom construction*, SIAM J. Appl. Math., 77 (2017), pp. 2093–2118.

- [3] W. BAO, W. JIANG, Y. WANG, AND Q. ZHAO, *A parametric finite element method for solid-state dewetting problems with anisotropic surface energies*, J. Comput. Phys., 330 (2017), pp. 380–400.
- [4] W. BAO AND Q. ZHAO, *A structure-preserving parametric finite element method for surface diffusion*, SIAM J. Numer. Anal., 59 (2021), pp. 2775–2799.
- [5] J. W. BARRETT, H. GARCKE, AND R. NÜRNBERG, *A parametric finite element method for fourth order geometric evolution equations*, J. Comput. Phys., 222 (2007), pp. 441–467.
- [6] J. W. BARRETT, H. GARCKE, AND R. NÜRNBERG, *Numerical approximation of anisotropic geometric evolution equations in the plane*, IMA J. Numer. Anal., 28 (2008), pp. 292–330.
- [7] J. W. BARRETT, H. GARCKE, AND R. NÜRNBERG, *The approximation of planar curve evolutions by stable fully implicit finite element schemes that equidistribute*, Numer. Methods Partial Differential Equations, 27 (2011), pp. 1–30.
- [8] J. W. BARRETT, H. GARCKE, AND R. NÜRNBERG, *Parametric finite element approximations of curvature-driven interface evolutions*, in Handb. Numer. Anal., vol. 21, Elsevier, 2020, pp. 275–423.
- [9] J. CAHN, *Stability, microstructural evolution, grain growth, and coarsening in a two-dimensional two-phase microstructure*, Acta Metall. Mater., 39 (1991), pp. 2189–2199.
- [10] J. W. CAHN AND J. E. TAYLOR, *Overview no. 113 surface motion by surface diffusion*, Acta Metall. Mater., 42 (1994), pp. 1045–1063.
- [11] U. CLARENZ, U. DIEWALD, AND M. RUMPF, *Anisotropic geometric diffusion in surface processing*, IEEE Visualization 2000, 2000.
- [12] K. DECKELNICK, G. DZIUK, AND C. M. ELLIOTT, *Computation of geometric partial differential equations and mean curvature flow*, Acta Numer., 14 (2005), pp. 139–232.
- [13] P. DU, M. KHENNER, AND H. WONG, *A tangent-plane marker-particle method for the computation of three-dimensional solid surfaces evolving by surface diffusion on a substrate*, J. Comput. Phys., 229 (2010), pp. 813–827.
- [14] J. EGGLESTON, G. MCFADDEN, AND P. VOORHEES, *A phase-field model for highly anisotropic interfacial energy*, Physica D: Nonlinear Phenomena, 150 (2001), pp. 91–103.
- [15] I. FONSECA, A. PRATELLI, AND B. ZWICKNAGL, *Shapes of epitaxially grown quantum dots*, Arch. Ration. Mech. Anal., 214 (2014), pp. 359–401.
- [16] D. W. HOFFMAN AND J. W. CAHN, *A vector thermodynamics for anisotropic surfaces: I. fundamentals and application to plane surface junctions*, Surface Science, 31 (1972), pp. 368–388.
- [17] W. HUANG, W. JIANG, AND Q. ZHAO, *A $\theta - L$ formulation-based finite element method for solving axisymmetric solid-state dewetting problems*, East Asian J. Appl. Math., 11 (2021), pp. 389–405.
- [18] W. JIANG, W. BAO, C. V. THOMPSON, AND D. J. SROLOVITZ, *Phase field approach for simulating solid-state dewetting problems*, Acta Mater., 60 (2012), pp. 5578–5592.
- [19] W. JIANG, Y. WANG, Q. ZHAO, D. J. SROLOVITZ, AND W. BAO, *Solid-state dewetting and island morphologies in strongly anisotropic materials*, Scr. Mater., 115 (2016), pp. 123–127.
- [20] W. JIANG AND Q. ZHAO, *Sharp-interface approach for simulating solid-state dewetting in two dimensions: A Cahn–Hoffman ξ -vector formulation*, Phys. D, 390 (2019), pp. 69–83.
- [21] W. JIANG, Q. ZHAO, AND W. BAO, *Sharp-interface model for simulating solid-state dewetting in three dimensions*, SIAM J. Appl. Math., 80 (2020), pp. 1654–1677.
- [22] Y. LI AND W. BAO, *An energy-stable parametric finite element method for anisotropic surface diffusion*, J. Comput. Phys., 446 (2021), p. 110658.
- [23] Z. LI, H. ZHAO, AND H. GAO, *A numerical study of electro-migration voiding by evolving level set functions on a fixed cartesian grid*, J. Comput. Phys., 152 (1999), pp. 281–304.
- [24] U. F. MAYER, *Numerical solutions for the surface diffusion flow in three space dimensions*, Comput. Appl. Math., 20 (2001), pp. 361–379.
- [25] W. W. MULLINS, *Theory of thermal grooving*, J. Appl. Phys., 28 (1957), pp. 333–339.
- [26] M. NAFFOUTI, R. BACKOFEN, M. SALVALAGLIO, T. BOTTEIN, M. LODARI, A. VOIGT, T. DAVID, A. BENKOUIDER, I. FRAJ, L. FAVRE, ET AL., *Complex dewetting scenarios of ultrathin silicon films for large-scale nanoarchitectures*, Sci. Advances, 3 (2017), p. 1472.
- [27] K. OURA, V. LIFSHITS, A. SARANIN, A. ZOTOV, AND M. KATAYAMA, *Surface science: an introduction*, Springer Science & Business Media, 2013.
- [28] A. P. SUTTON AND R. W. BALLUFFI, *Interfaces in crystalline materials*, Clarendon Press, 1995.
- [29] J. E. TAYLOR, *Mean curvature and weighted mean curvature*, Acta Metall. Mater., 40 (1992), pp. 1475–1485.
- [30] J. E. TAYLOR AND J. W. CAHN, *Linking anisotropic sharp and diffuse surface motion laws via gradient flows*, J. Stat. Phys., 77 (1994), pp. 183–197.
- [31] C. V. THOMPSON, *Solid-state dewetting of thin films*, Annu. Rev. Mater. Res., 42 (2012), pp. 399–434.

- [32] Y. WANG, W. JIANG, W. BAO, AND D. J. SROLOVITZ, *Sharp interface model for solid-state dewetting problems with weakly anisotropic surface energies*, Phys. Rev. B, 91 (2015), p. 045303.
- [33] A. WHEELER, *Cahn–Hoffman ξ -vector and its relation to diffuse interface models of phase transitions*, J. Stat. Phys., 95 (1999), pp. 1245–1280.
- [34] H. WONG, P. VOORHEES, M. MIKSIK, AND S. DAVIS, *Periodic mass shedding of a retracting solid film step*, Acta Mater., 48 (2000), pp. 1719–1728.
- [35] G. WULFF, *Zur frage der geschwindigkeit des wachstums und der auflösung der krystallflächen*, Z. Kristallogr, 34 (1901), pp. 449–530.
- [36] L. XIA, A. F. BOWER, Z. SUO, AND C. SHIH, *A finite element analysis of the motion and evolution of voids due to strain and electromigration induced surface diffusion*, J. Mech. Phys. Solids, 45 (1997), pp. 1473–1493.
- [37] Y. XU AND C.-W. SHU, *Local discontinuous Galerkin method for surface diffusion and Willmore flow of graphs*, J. Sci. Comput., 40 (2009), pp. 375–390.
- [38] J. YE AND C. V. THOMPSON, *Mechanisms of complex morphological evolution during solid-state dewetting of single-crystal nickel thin films*, Appl. Phys. Lett., 97 (2010), p. 071904.
- [39] Q. ZHAO, W. JIANG, AND W. BAO, *A parametric finite element method for solid-state dewetting problems in three dimensions*, SIAM J. Sci. Comput., 42 (2020), pp. B327–B352.
- [40] Q. ZHAO, W. JIANG, AND W. BAO, *An energy-stable parametric finite element method for simulating solid-state dewetting*, IMA J. Num. Anal., 41 (2021), pp. 2026–2055.